Fall 12-16-2016

Numerical Computation of Transient Response of 2D Wedge Impact

Naresh Kumar Koyyapu
University of New Orleans, naresh.kk@outlook.com

Numerical Computation of Transient Response of 2D Wedge Impact

A Thesis

Submitted to the Graduate Faculty of the
University of New Orleans
in partial fulfillment of the
requirements for the degree of

Master of Science
in
Engineering
Naval Architecture and Marine Engineering

by

Naresh Kumar Koyyapu

B.E. Andhra University, 2008
M.Tech. Andhra University, 2012

December, 2016

DEDICATION

To my lovely wife, Gayatri, for all of her support . . .

To my parents and my brother for their support . . .

ACKNOWLEDGEMENTS

First of all, I sincerely thank my advisor, Dr. Brandon M. Taravella, Associate Professor of Naval Architecture and Marine Engineering at the University of New Orleans, who always gave valuable guidance and suggestions for my thesis. This thesis would not have taken this form without his valuable feedback and time.

I would also like to thank my committee members Dr. Lothar Birk, Associate Professor and Chair in the Department of Naval Architecture and Marine Engineering (NAME) and Dr. Xiaochuan(Vincent) Yu, Assistant Professor of NAME for reviewing my thesis.

Special thanks to Dr. Nikolas Xiros, Associate Professor and Dr. Christine Ikeda, Assistant Professor of NAME, Dr. Kazim M. Akyuzlu, Professor of Mechanical Engineering at the University of New Orleans for their continuous encouragement during my studies at the University of New Orleans.

I express my gratitude to the Louisiana Board of Regents (Contract # LEQSF(2015-18)-RD-B-09) for funding the research.

Lastly, I would like to thank Mr. Krishna M Karri, Project Manager at Technology Associates Inc. for his valuable comments on my thesis and also extend my deepest thanks to my wife Gayatri, and my brother Suresh for their support and encouragement.

TABLE OF CONTENTS

LIST OF FIGURES

NOMENCLATURE

Symbol	Units	Description
ρ	$slugs/ft^3$	density
ω	rad/sec	excitation frequency
Ω_f	rad/sec	characteristic flexural frequency
Ω_r	rad/sec	characteristic rigid-body frequency
β	$degrees$	Deadrise angle
E	ksi	Modulus of elasticity
L	$inches$	Length
L_i	$inches$	Length of each element
B	$inches$	Maximum beam
D	$inches$	Maximum depth
I	$inch^4$	Moment of inertia
F	lbs/ft	Force
m	$slugs/ft$	mass
p	lbs/ft^2	Pressure
w	$inches$	deflection
$\dot{w}$	ft/sec	velocity
$\ddot{w}$	ft/sec^2	acceleration
z_c	$inches$	hydrodynamic wetted breadth
Z_{ch}	$inches$	chine breadth
C_{pi}	-	Pressure distribution
V	ft/sec	Impact velocity

ABSTRACT

The diverse applications of advanced marine craft ascribed to their high speed and technological advancements has led to the use of stronger and lighter metals in such crafts. High speed, in effect also increases slamming loads as higher speed increases frequency of wave encounter while operating in waves. The present study is limited to wedge impact models. Fundamentally, the study is thus about two-dimensional (2D) wedge impact in water. In an attempt to predict the structural response to impact hydrodynamic force, a beam element based finite element (FE) computer program is written and the results of the code are presented in the thesis. A computational tool is developed to predict the transient elastic response of a 2D wedge under impact force using two different numerical methods. Both explicit and implicit numerical schemes have also been studied in order to apply to the present work. Explicit forth order Runge-Kutta (RK4) method and implicit Newmark-β (NB) method have been used in the present work. Coupling effects between excitation and response are ignored in the present numerical computations. Both the numerical schemes are validated using simple static solution and also modal expansion technique. The hydrodynamic pressure distribution along the bottom of a 20° deadrise wedge is computed using a flat cylinder theory (Vorus, 1996). An impact velocity of 9.51 *ft/sec* is used and two different structural boundary conditions are considered in the present analysis. In addition, three different plate thicknesses have been used in the analysis and the results are compared against each other. Stability of the results is tested using node variation test. The results have shown that maximum deflection is around 8 times more for a pinned-pinned beam when compared to clamped-clamped beam. Also, lower plate thickness yielded very significant deflections in both the boundary conditions.

Keywords: *2D wedge, excitation, impact, planing, deflection, slamming*

CHAPTER 1
INTRODUCTION

A ship hull is exposed to different load environments while operating at sea. Of them, slamming loads are particularly significant in both large commercial marine vessels and high speed ships. Among several categories of vessels, the attention of this thesis is paid mainly to the slamming in high speed planing vessels. A brief literature review is presented in this chapter about the available theories to compute the peak impact pressures. Some light is also shed on the concept of hydroelasticity for the sake of completeness of the study. The goal of the present study including scope of work and also the proposed method is presented in the following sections.

1.1 Review

The structural strength is an important aspect in the design of ships and any offshore structure. Any ship or offshore structure shall be designed to withstand the static and dynamic forces acting on them. These forces could originate from a variety of sources, such as low and high frequency hydrodynamic wave loads, impact loads due to slamming and green water, steady impact force on high speed planing hulls, and liquid sloshing in tanks, etc. Moreover, the elastic response of a structure to such loads for short periods of time can have significant effect on fatigue life of the structure. The *elastic* response of a structure under the action of water (*hydro*) is a subcategory of Fluid Structure Interaction (FSI) problems and studied as *Hydroelasticity* [1]. This concept has gained impetus in both marine and offshore industry in this 21^{st} century in order to gain some insight, which led to the development of several techniques *viz.,* numerical and computational methods.

Ships, by and large are used to carry cargo in liquid, bulk and containerized form and also to transport passengers. In addition, they also form an integral part of nations' military and security forces. A ship hull is exposed to different load environments while operating at sea. In heavy seas, when the relative velocity of the ship's bottom and sea surface is large, a ship tends to 'slam' at the forefoot while she reenters into water. *Slamming*, thus is a violent impact of the ship against water.

Slamming introduces impulsive loading which excite hull vibrations and locally damage the ship due to overstress. The ship may also suffer fatigue damage due to repeated slamming. In addition, slamming introduces transient hull vibration known as *whipping* resulting in vibratory stresses.

In recent days, novel hull form developments led to an improvement in speed with reduced resistance/drag, lowered power demand, minimized the fuel consumption, and also improved the seakeeping behaviour. However, higher speeds also make the crafts susceptible to slamming. With the growing demand for increased speed to the vessels deployed for various missions, numerous advanced hull forms have evolved. These advanced hull forms fundamentally differ from each other in terms of the source for the generation of hydroynamic lift. Complex hydrodynamic interactions related to intricate design characteristics further made the operation of such high speed craft extremely difficult in heavy seas.

High speed crafts usually attain an aft trim during their operation such that the bow portion is lifted clear of the water surface. The occurrence of slamming to these crafts is eminent owing to their high speed, which increases the frequency of wave encounter while operating in waves. Much attention is paid to the planing crafts in the present work. It was reported for planing vessels that slamming introduces very large upward accelerations at very frequent intervals even in moderately rough seas [2].

A considerable portion on the planing hull research has been evolved as impact studies on wedges. A wedge section represents a typical transverse hull section in a planing vessel and are used to study the flow under impacts. The flow past a planing hull is thus treated equivalent to flow due to water entry of a 2D body with changing form and downward velocity, V. So, wedge drop tests are being used as basis to gain some insight into problems associated with high speed planing vessels.

The present report is limited to the simple wedge impacts. In the case of planing hulls, the hydrodynamic lift is due to bottom positive pressures. The high speed also makes the craft

subject to slamming loads. The high pressure peaks are not only time and space dependent but also localized, and hence the force impulse is important for the structural response. These impact loads will induce significant stresses in the structure of the craft and also change with time as the craft moves forward. The frequent exposure to impact loads further accelerates the fatigue failures of these hulls even when the impact load is small. In addition, as the impact duration is very short, hydro-elastic effects prevail [3]. The present study is conducted to understand the transient response of the structure in both a qualitative and quantitative manner.

Numerous two-dimensional linear as well as non-linear theories have been evolved to study slamming, although it is strictly a three-dimensional non-linear problem. The assumptions made by several authors including two dimensionality and linearization gave some important results which have practical significance. Von Karman [4] pioneered the classical work to study theoretical water impact (slamming) on seaplanes during landing. He idealized the impact as a 2-D wedge entry problem on the calm-water surface. Further assumptions in his momentum impact theory include the impact is so rapid, and hence water surface elevation is very small during impact and gravity effects can be neglected. However, the added mass and impact load are underestimated particularly for small deadrise angles in von Karman's impact theory which is based on momentum conservation.

Later, Wagner [5] derived another realistic impact theory. He assumed that the flow under the wedge can be approximated by the flow around an expanding flat plate in uniform flow with velocity. In his analytical treatment, he used time integral of the spatial derivative of velocity potential, ϕ in the *y-direction*. The impact pressure is derived using Bernoulli's equation. The peak impact pressure using Wagner's theory gave some interesting and conservative estimates which are in pratical use even today.

Vorus [6] presented a flat cylinder hydrodynamic theory to analyze impact loads on typical sections of vessels operating in waves and also to study hydrodynamics of steady planing in calm water. In his work, he specified a uniform first-order geometric linearity and all boundary condi-

tions are satisfied on the horizontal axis in the limit of flatness. In his hydrodynamic theory, Vorus retained the hydrodynamic nonlinearity of the exact formulation. His theory also achieved uniform geometric linearity in the flatness limit accompanied by uniform hydrodynamic nonlinearity. He proposed discretization of the general theory for numerical analysis. The hydrodynamic loads in this work are predicted based on Vorus' theory and forms an input to the numerical code in the present work.

Faltinsen [7] made a comparison between theoretical and experimental work on wetdeck slamming in catamaran. His experiment results of structural strain and displacement strongly confirmed with hydroelastic orthotropic plate theory. Later in the year 1999, he mentioned about the significance of hydroelasticity in terms of ratio between the wetting time of the structure and the greatest wet natural period of the stiffened plating. He analyzed wedge-shaped cross sections of aluminum catamaran using generalized Wagner's theory and coupled with the orthotropic plate theory for three-dimensional flow effects. Korobkin *et al* [8] developed a hydroelastic method. The structure of a wedge-shaped body was described using finite elements that impacts a calm free surface vertically at moderate velocity. Finite Element Method (FEM) was used to couple the structure with the fluid in order to calculate hydroelastic response and added masses for different discretizations.

A recent study was also conducted on the hydroelastic impact entry and exit of a wedge by Piro and Maki [9]. In their computational approach, they used a loosely coupled Fluid-Structure Interaction (FSI) solver to couple a finite element model to a Computational Fluid Dynamics (CFD) model. Also, Piro [10] with his doctoral research studies on slamming events examined the role of hydroelasticity. He concluded in his studies on the elastic wedge entry and exit that the structural deflection on exit could be larger than during impact.

In a related work, Nabanita [11] studied the response behavior of flexible rectangular isotropic plate under transient impact loads. In her study she assumed a one-way coupling between the fluid and structure. Also she studied the time dependent impact loads as the effect of

moving loads on structures.

Fiber composites have also found their application in high speed crafts owing to their high strength to weight ratio. In addition, alternate available materials have been looked after like Aluminum. Recently, Ikeda *et al* conducted free-falling wedge drop experiment to study the effects of slamming on the bottom of high-speed aluminum planing craft. [12]. All the developments in the experimental work related to wedge impact studies can be found in Ikeda [13].

Jian and Grenestedt [14] analytically studied the deformation of boat hull bottom panels during the initial phase of slamming using a linear elastic Euler-Bernoulli beam. The slamming pressure has been modeled as a high intensity peak followed by a lower constant pressure (two-step load). The problem is solved using a Fourier sine integral transformation in space and a Laplace-Carson integral transformation in time.

Volpi *et al* [15] developed CFD/FE FSI (Computational Fluid Dynamics/Finite Element Fluid-Structure Interaction) code to analyze hydrodynamic and slamming response and validated using full-scale experiments on a fully instrumented high speed planing hull. The structural problem is solved by ANSYS for displacements, strains and stresses. The Newmark time integration method has been used to solve the FE equations.

In principle, the three-dimensional treatment of slamming phenomenon became a major part in today's research. The structural design being a critical aspect in the design phase of planing hull, the evaluation of peak impact pressures and the structural response to such impacts cannot be ignored. Perhaps in order to make progress towards more challenging three-dimensional hydroelastic problems, one must be prudent to understand the complications involved with simplifying assumptions such as two dimensionality. Thus, the present work although limited to study the structural response of two-dimensional wedge hull under impacts using Finite Element model. This was attempted with the hope that it will assist in improving our capability on similar hydroelastic slamming problems.

The bottom plating of the 2D wedge section can be treated as a two-dimensional beam with its one end supported at chine and the other end at the keel. Two different boundary conditions namely pinned-pinned (PP) and clamped-clamped (CC) are considered. The hydrodynamic loads are applied at nodes based on wetted breadth of the section. This is explained more elaborately in Chapter 2. The hydrodynamic pulse loads are acted upon the section for a very finite interval. In order to generate the response to such time dependent force, a numerical code is written to calculate the deflection of the beam. Two numerical schemes are used in the numerical code. The ideal method to calculate the deflection is to calculate the high frequency transient response of the beam. The methodology and the working principle of the code is discussed in Chapter 3. The code has been validated and verified using modal expansion technique and also simple static solutions which can be seen in Chapter 4. The results are discussed in Chapter 5. Finally conclusions and the future work are highlighted in Chapter 6.

1.2 Purpose, Motivation and Objective of Study

High speed crafts experience significant bottom pressures while underway. The structure of the craft tends to deflect in response to impact peak pressures for short period of time. The deflection of hull plating alters the surrounding pressure field in a complicated manner which inturn has an effect on the structural response. In order to solve the implicit equation of motion, the velocity or deflection should be known at an instant under impact loads. Then, we can estimate the structural response of the hull in the subsequent time steps.

The three dimensionality and the instantaneous variation of hydrodynamic pressure further adds complexity to predict the response. An attempt to estimate the response of the hull to planing pressures with simplifying assumptions has been made in the present work.

The goal is to formulate a computer code and numerically compute the response under a given input force using finite element (FE) discretisation as a two-dimensional beam element. Also, a qualitative and quantitative study is made to validate the accuracy of the code.

1.3 Proposed method

In order to understand the structural behavior under the action of a time dependent excitation, the 3D hull model needs simplification. A transverse section of a three dimensional hull essentially becomes two dimensional and the aspect ratio is assumed high. The bottom panel in effect also becomes two-dimensional and designated as beam. The hydrodynamic excitation can then be treated as a distributed load along the length of the beam. The variation in hydrodynamic loading is accounted through a change in the wetted length as the section is immersed in the water. Both the explicit and implicit numerical methods are used in the computer program. This is explained more in detail in Chapter 2 and Chapter 3.

1.4 Scope of the Study

The scope of the present study is to develop and validate an algorithm to compute the transient elastic response of a two dimensional wedge under free impact. A general study is also conducted on the explicit and implicit schemes to understand their applicability to the problem among the available numerical methods. The scope also includes comparison of deflection with two different boundary conditions in addition to response comparison with three different plate thicknesses for a test wedge geometry.

CHAPTER 2
BACKGROUND

An overview of the problem and the background work is presented in this chapter. A slender planing hull with a wedge-shaped cross section is considered. The assumptions and the simplifications in the present work are outlined.

2.1 Hull Particulars

The geometry of transverse section of the hull is shown in Figure 2.1. The hull bottom panel of the prismatic model is considered for the present work. The response of such plate panel under impulse loads constituted a major part in the present study. However, the three-dimensional planar panel required further simplification. The isometric view of part of the hull is illustrated in Figure 2.2 with the front and rear plating removed. The bottom panel alone is then treated as two-dimensional beam of infinite length *i.e.,* assumed high aspect ratio. Essentially, the problem is to analyze a two-dimensional beam subject to hydrodynamic impulse loading.

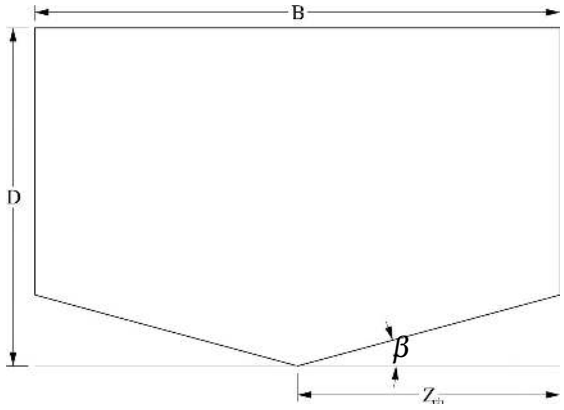

Figure 2.1: Model wedge hull transverse section

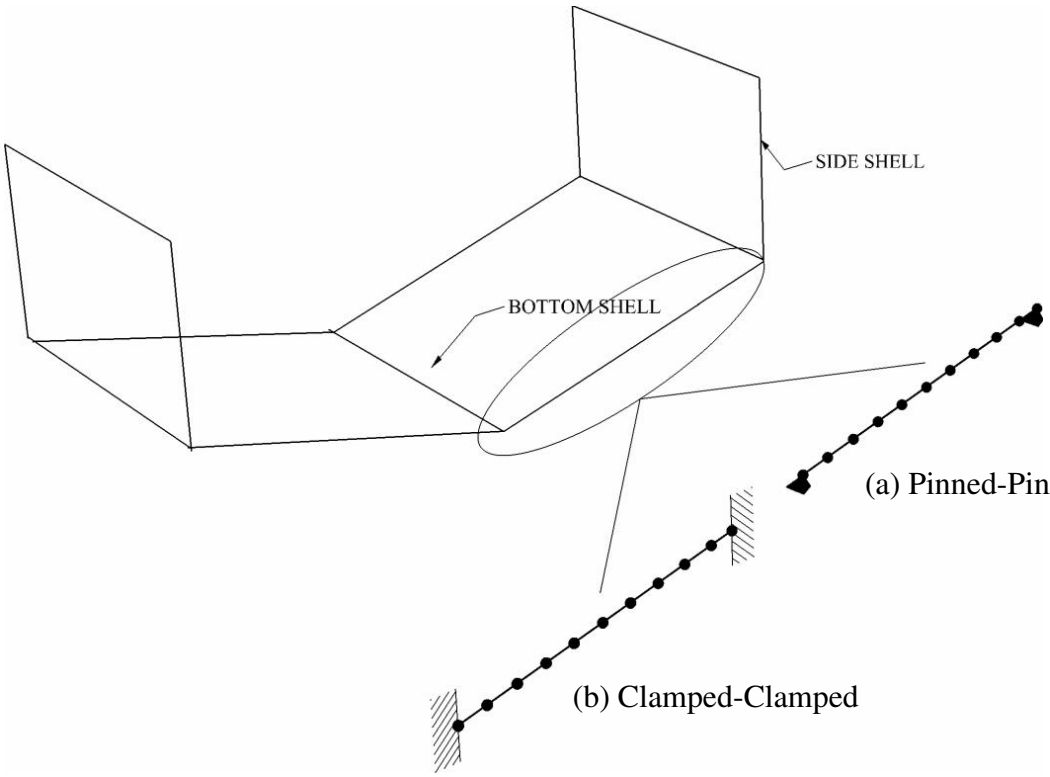

Figure 2.2: Isometric model showing hull panels

The present method has discrete finite elements along the length. In fact, the length is divided into segments and the ends of each segment are called nodes. Two different end conditions were considered (See Figure 2.2 (a) & (b)).

2.2 Equation of motion

The equation of motion in matrix form can be represented as:

$$[\mathbf{F}(t)] = [\mathbf{M}(t)]\,[\ddot{w}(t)] + [\mathbf{B}]\,[\dot{w}(t)] + [\mathbf{K}]\,[w(t)] \tag{2.1}$$

where, $[\mathbf{F}(t)]$ is the external force vector (2N$\times$1) which includes hydrodynamic and hydrostatic forces. $[\mathbf{M}(\mathbf{t})]$ is the mass matrix (2N$\times$2N) including physical mass and hydrodynamic added mass. The added mass is a function of time and thus the mass matrix also depends on time. $[\mathbf{B}]$ is the structural damping (2N$\times$2N) of the system (hydrodynamic damping neglected), $[\mathbf{K}]$ is structural stiffness matrix (2N$\times$2N) of the system and N indicates number of nodes.

Equation (2.1) is solved using two different numerical schemes namely Runge-Kutta (RK4) method and Newmark-β (NB) method. On one end, Runge-Kutta method is self-starting and fourth order accurate. Thus, the solution at the next time step is obtained based on the current time step and hence explicit. On the other, Newmark-β method is implicit and second order accurate. A comparison of the results between both the methods using two different boundary conditions is shown in Chapter 5.

The methodology and algorithm of the code is explained in detail in the next chapter.

CHAPTER 3
METHODOLOGY

The response of the structure under sudden nonperiodic excitation can be treated as an impulse problem. Such a response to sudden nonperiodic excitation is called transient response. Further the hydrodynamic pressure under the wedge changes quite often and hence cannot be expressed as simple functions. Also, the hydrodynamic pressure is non-linear in space and time. In addition, the response also depends on initial conditions of the system. Thus, in order to solve such time dependent problems, numerical methods must be used. Of them, most popular fourth order Runge-Kutta method (abbreviated as RK4 method) and Newmark-β (NB method), are used currently in the code to solve the differential equation in a progressive manner.

3.1 Methodology

The structure of the computer code and the working algorithm is presented in this chapter. The code is constructed and integrated in accordance with the well established finite element modelling principles. The code reads the input force from an external code which generates the hull pressures at certain instants of time during the impact. This is used as an input excitation force to generate the response. The flowhart is shown in figure 3.1. The input variables are read from a data file (input). The mass, stiffness and damping matrices are generated based on a data file. The mass matrix is then updated based on the number of wetted nodes after calculating the added mass at the nodes during each time step. The matrices are then reshaped based on the end conditions of the beam. Nodal force is evaluated using pressure obtained from the hydrodynamic code. A numerical method is used to solve for nodal deflection, velocity and acceleration at each time step.

3.2 Finite Element Modelling

The 2D dimensional wedge is modelled as a beam having length L and divided into n elements *i.e., N nodes*. It was considered that the beam possess uniform stiffness. Also mass moment of inertia is considered but deformation due to shear has been neglected as effective shear is small for a plate.

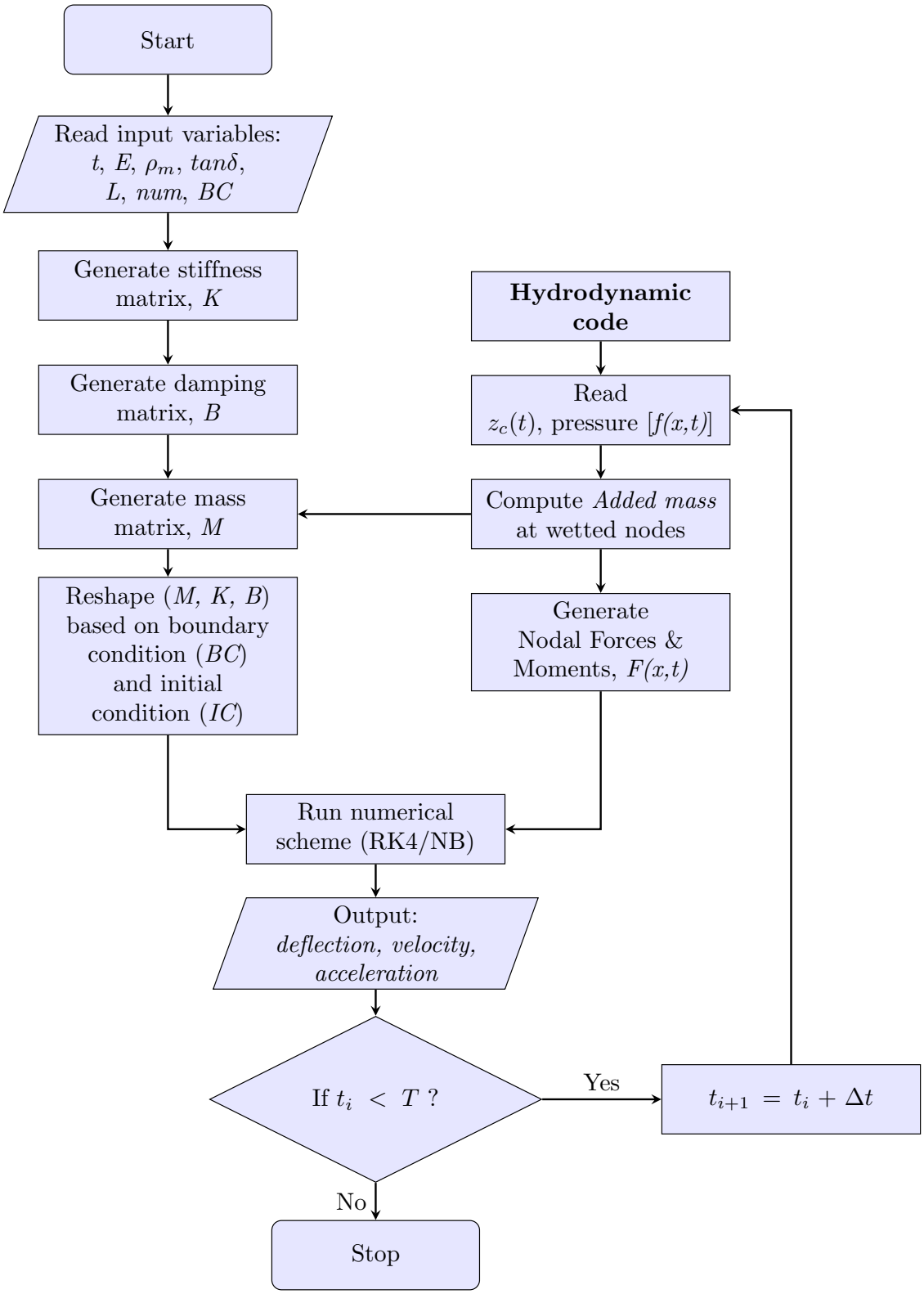

Figure 3.1: Program Flowchart

Global mass matrix, $[\mathbf{M}]$ is obtained from the following:

$$[\mathbf{M}]_{\mathbf{2N}\times\mathbf{2N}} = \begin{pmatrix} m_j & 0 & 0 & 0 & \dots & \dots & 0 & 0 \\ 0 & I_j & 0 & 0 & \dots & \dots & 0 & 0 \\ 0 & 0 & m_{j+1} & 0 & \dots & \dots & 0 & 0 \\ 0 & 0 & 0 & I_{j+1} & \dots & \dots & 0 & 0 \\ \dots & \dots & \dots & \dots & \ddots & \dots & 0 & 0 \\ \dots & \dots & \dots & \dots & \dots & \ddots & 0 & 0 \\ 0 & 0 & 0 & 0 & 0 & 0 & m_N & 0 \\ 0 & 0 & 0 & 0 & 0 & 0 & 0 & I_N \end{pmatrix}$$

where, m_j represents the node mass including the beam element mass and added mass when the nodes are wet ($j = 1, N$). I_j represents the node mass moment of inertia, which includes the beam element mass and added mass at the nodes while the nodes are wet ($j = 1, N$).

3.2.1 Added Mass

The added mass of a 2D wedge is calculated based on the added mass equivalent to that of a flat plate.

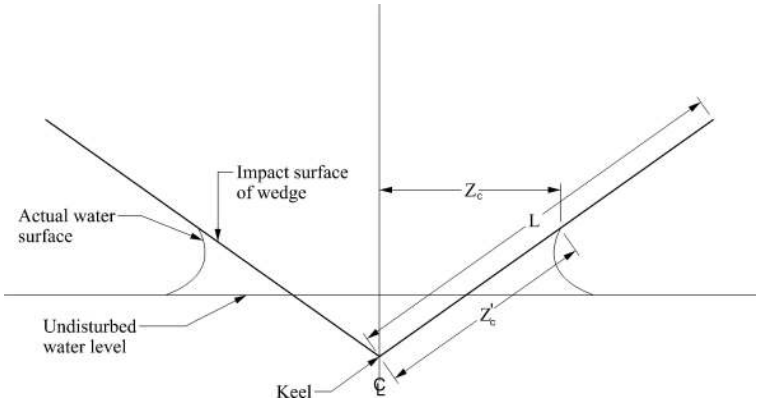

Figure 3.2: Wedge approximation

The added mass, $M_a(t)$ is calculated as:

$$M_a(t) = \frac{1}{2}\pi\rho z_c(t)^2 \tag{3.1}$$

where, ρ = water density, $z_c(t)$ = hydrodynamic wetted breadth (function of time)

The beam element stiffness matrix (for the i^{th} element) is a symmetric matrix about the leading diagonal and given as:

$$\mathsf{K_i} = \frac{EI}{l^3}\begin{pmatrix} 12 & 6l & -12 & 6l \\ 6l & 4l^2 & -6l & 2l^2 \\ -12 & -6l & 12 & -6l \\ 6l & 2l^2 & -6l & 4l^2 \end{pmatrix}$$

where, l represents i^{th} element length. Elastic rigidity (EI) is constant for the entire beam as the beam is assumed of same material and also possess uniform area moment of inertia throughout due to constant plating thickness on the hull bottom.

Global stiffness matrix, $[\mathbf{K}]$ is obtained as follows:

$$[\mathbf{K}]_{\mathbf{2N\times 2N}} = \frac{EI}{l^3}\begin{pmatrix} 12 & 6l & -12 & 6l & 0 & 0 & \dots & \dots & 0 & 0 \\ 6l & 4l^2 & -6l & 2l^2 & 0 & 0 & \dots & \dots & 0 & 0 \\ -12 & -6l & 12+12 & -6l+6l & 0+(-12) & 0+(6l) & \dots & \dots & 0 & 0 \\ 6l & 2l^2 & -6l+6l & 4l^2+4l^2 & 0+(-6l) & 0+2l^2 & \dots & \dots & 0 & 0 \\ 0 & 0 & -12 & -6l & \ddots & \dots & \dots & \dots & 0 & 0 \\ 0 & 0 & 6l & 2l^2 & \dots & \ddots & \dots & \dots & 0 & 0 \\ \dots & \dots & \dots & \dots & \dots & \dots & \ddots & \dots & \dots & \dots \\ \dots & \dots & \dots & \dots & \dots & \dots & \dots & \ddots & \dots & \dots \\ 0 & 0 & 0 & 0 & 0 & 0 & \dots & \dots & 12 & \dots \\ 0 & 0 & 0 & 0 & 0 & 0 & \dots & \dots & \dots & 4l^2 \end{pmatrix}$$

3.2.2 Visco-elastic model (Structural Damping)

Structural damping is calculated based on Voigt Kelvin model. Voigt Kelvin model represents the structural stiffness and damping with a spring and dashpot respectively in parallel [16].

$$\sigma(t) = E\varepsilon(t) + \nu\frac{d\varepsilon(t)}{dt} \tag{3.2}$$

Further simplification leads to: $\nu = \frac{E}{\omega}tan\delta$ where, $tan\delta$ represents damping.

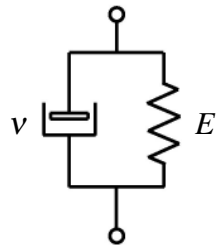

Figure 3.3: Voigt Kelvin Model
(Image Courtesy: [17])

Global damping matrix, $[\mathbf{B}]$ is obtained as follows:

$$[\mathbf{B}]_{\mathbf{2N}\times\mathbf{2N}} = tan\,\delta * [\mathbf{K}]_{\mathbf{2N}\times\mathbf{2N}}$$

The equation of motion for forced vibration is:

$$\mathbf{F}(t) = \mathbf{M}\ddot{w}(t) + \mathbf{B}\dot{w}(t) + \mathbf{K}w(t) \tag{3.3}$$

where, $w(t)$ is deflection, $2N\times 1$.

Equation (3.3) is solved using two numerical schemes namely fourth order Runge-Kutta (RK4) method [18] and Newmark-β method [19].

RK4 method is one of the most powerful numerical schemes to integrate ordinary differential equation. This method is self-starting and results in good accuracy. In this method,

the second-order differential equation is first reduced to two first-order equations.

Equation (3.3) can be rewritten as:

$$\ddot{w}(t) = \frac{1}{\mathbf{M}}\Big(\mathbf{F}(t) - \mathbf{B}\,\dot{w}(t) - \mathbf{K}\,w(t)\Big) = f(w, \dot{w}, t) \tag{3.4}$$

In RK4 method, the solution for the next time step shall be obtained from the current time step based on the following recurrence relations :

$$w_{i+1} = w_i + \frac{\Delta t}{6}\left[\dot{W}_1 + 2\dot{W}_2 + 2\dot{W}_3 + \dot{W}_4\right] \tag{3.5}$$

$$\dot{w}_{i+1} = \dot{w}_i + \frac{\Delta t}{6}\left[f_1 + 2f_2 + 2f_3 + f_4\right] \tag{3.6}$$

where, f_1, f_2, f_3, f_4 are obtained using (3.4) at T_1, T_2, T_3, T_4 respectively with corresponding W and $\dot{W}$ values. W and $\dot{W}$ at each corresponding time step are calculated as:

$$\begin{aligned}
&T_1 = t_i, \quad W_1 = w_i, \quad \dot{W}_1 = \dot{w}_i; \\
&T_2 = t_i + \Delta t/2, \quad W_2 = w_i + \dot{W}_1\frac{\Delta t}{2}, \quad \dot{W}_2 = \dot{w}_i + f_1\frac{\Delta t}{2}; \\
&T_3 = t_i + \Delta t/2, \quad W_3 = w_i + \dot{W}_2\frac{\Delta t}{2}, \quad \dot{W}_3 = \dot{w}_i + f_2\frac{\Delta t}{2}; \\
&T_4 = t_i + \Delta t, \quad W_4 = w_i + \dot{W}_3\Delta t, \quad \dot{W}_4 = \dot{w}_i + f_3\Delta t
\end{aligned}$$

Although the method is relatively simple to execute as a good computer program, the method experiences occasional difficulties [20]. So the time step size has to be chosen judiciously to avoid numerical breakdown and thus RK4 method exhibits a form of conditional stability. This is important for stiff ordinary differential equations. Also if the magnitudes are very large, the solution does not converge. Numerical breakdown can also occur when the number of elements are large which increase the stiffness of the system and leads to a stiff differential equation.

The Newmark-β (NB) method is a time-integration method used to solve differential equa-

tions. This method is widely used in numerical evaluation of the dynamic response of structures.

$$\dot{w}_{i+1} = \dot{w}_i + (1-\gamma)\,\Delta t\,\ddot{w}_i + \gamma\,\Delta t\,\ddot{w}_{i+1} \tag{3.7}$$

$$w_{i+1} = w_i + \Delta t\,\dot{w}_i + \Delta t^2\left(\frac{1}{2} - \beta\right)\ddot{w}_i + \Delta t^2\,\beta\,\ddot{w}_{i+1} \tag{3.8}$$

where, γ and β are parameters associated with the quadrature scheme.

Using Equations (3.3), (3.7) and (3.8), the equilibrium equation at t_{i+1} can be rewritten as:

$$\begin{aligned}
&[M + \gamma\Delta t\,B + \beta\,\Delta t^2\,K]\ddot{w}_{i+1} \\
&= \quad F_{i+1} - B[\dot{w}_i + (1-\gamma)\,\Delta t\,\ddot{w}_i] - K[w_i + \Delta t\,\dot{w}_i + \left(\frac{1}{2} - \beta\right)\Delta t^2\,\ddot{w}_i]
\end{aligned} \tag{3.9}$$

The above system of equations are solved for $\ddot{w}_{i+1}$. The result is then substituted in equations (3.7) and (3.8) to obtain $\dot{w}_{i+1}$ and w_{i+1}. In Newmark's family of methods, the average constant acceleration scheme (γ = 1/2; β = 1/4) is used in the present work. The average constant acceleration method is unconditionally stable with asymptotically the highest accuracy.

The computer program is validated using modal expansion technique for steady state and also using simple static solutions. The code validation is discussed in Chapter 4.

3.3 Impact pressure

Impact pressure is calculated using hydrodynamic code based on Vorus flat cylinder theory [6]. The boundary value problem formulated by Vorus is shown in figure 3.4. The impact flow is forced to separate at chine, Z_{ch}. The vertically downward velocity of the cylinder, *V(t)*, is specified, so that the undisturbed water surface at time t above the keel, $Y_{wl}(t)$, is the integral of *V(t)*. The z-axis lies in the water surface and the y-axis lies on the cylinder vertical centerplane. The jet "spray root," with coordinate $z_b(t)$, advances rapidly outward along the contour, followed closely behind $z_c(t)$, the point of zero contour dynamic pressure. The cylinder is made flat by collapsing the cylinder and free-surface contours to the z-axis for the purpose of satisfying boundary conditions. A detailed

information about the theory can be found in literature [6]. The side hull pressure distribution at the i^{th} element center point of the k^{th} strip is given by the Bernoulli equation:

$$C_{pi} = 2z_{ct}[V_j(b-1) - \phi_i + w_i\zeta_i] + 1 - {w_i}^2 \tag{3.10}$$

with the potential in Eqn. (3.10) as:

$$\phi_{nz-i} = \phi_{nz-i+1} - \frac{1}{2}\sum_{j=1}^{nz-i} \Delta\zeta_j[w_{nz-j} + w_{nz-j+1}] \tag{3.11}$$

for $\phi_{nz} = 0$ and $\Delta\zeta_i = \zeta(nz-i+1) - \zeta(nz-i)$.

where, V_j is the jet velocity, w is the tangential perturbation velocity. Also, zero-pressure point velocity, $z_{ct} = \dfrac{z_{bt}}{b}$ and b is the ratio of jet head velocity to zero-pressure point velocity with z_{bt} being the jet head offset velocity; ζ is the nondimensional offset coordinate z on $z_c(t)$ and nz indicates discretization points.

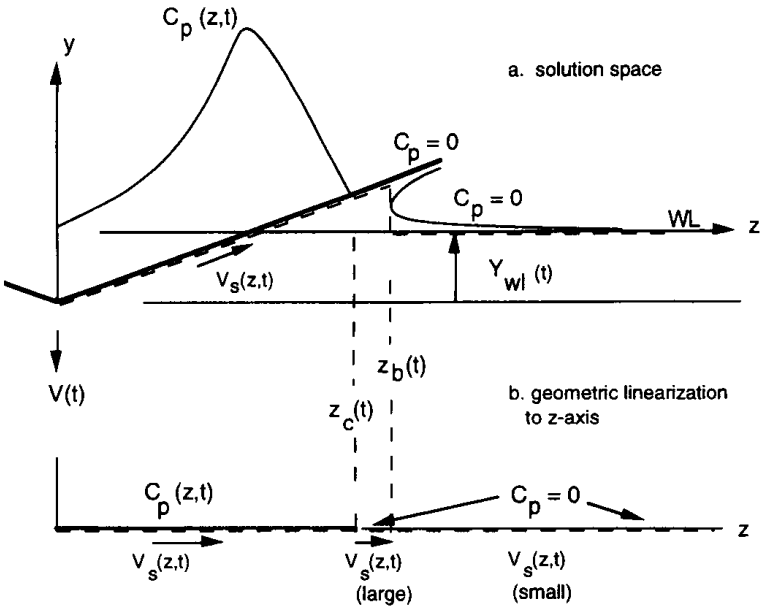

Figure 3.4: Physical approximation
(Image courtesy: Vorus [6])

The major contribution from the Vorus work is the the nonzero gravity formulation which indicates that the zero hydrostatic pressure datum should not be at the intersection of the hull contour and the undisturbed free-surface elevation. The hydrodynamic pressure is computed using Vorus theory in the present work. However, the present numerical code doesnot impose any restrictions pertaining to the computation of hydrodynamic pressure. Any hydrodynamic theory can be selected and combined with the code to predict the structural response.

3.4 Nodal Force Evaluation

The free fall impact pressure is obtained from the hydrodynamic code as discussed in the previous section. The force at each node is evaluated as discussed in this section.

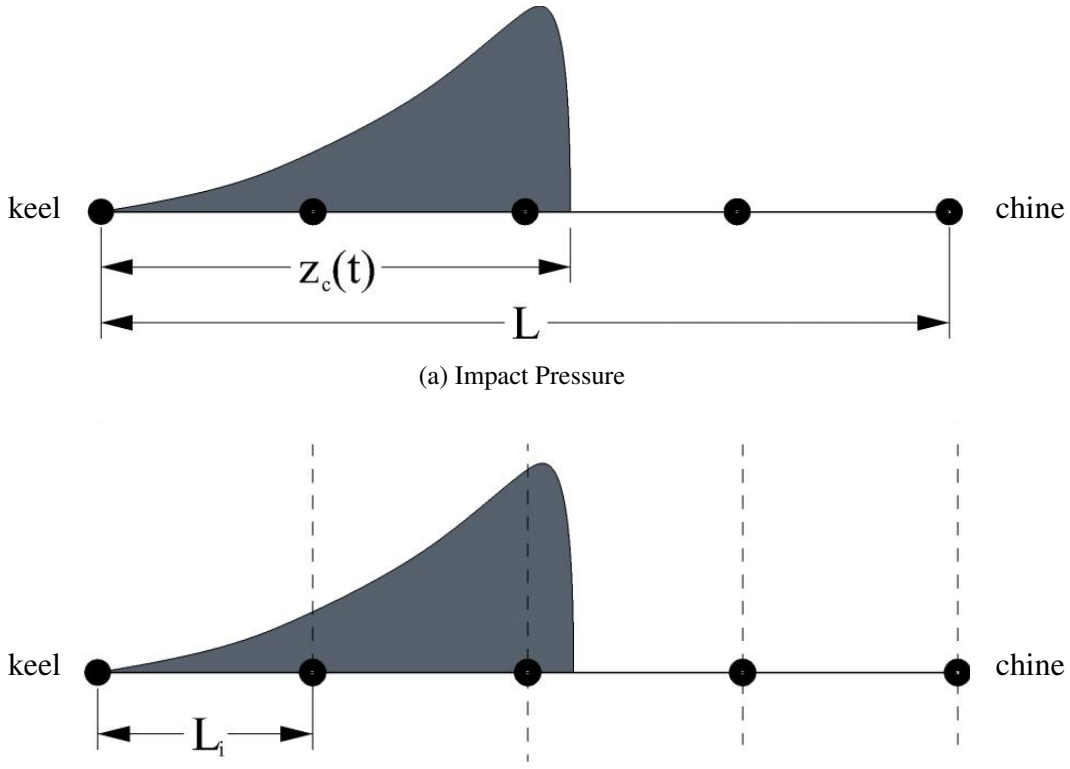

(a) Impact Pressure

(b) Intermediate nodes (*dashed lines*)

Figure 3.5: Pressure to Nodal Force/Moment Evaluation: Step-1

A discretized plate panel of length L is shown with a typical impact pressure profile in figure 3.5a. Impact pressure is a result of a wedge form hull panel interacting with a water body.

Several node points are used in the analysis although the RK4 method breaksdown beyond 5 nodes with 0.1 *ms* which is not the case with NB method. Distance between successive nodes is measured as L_i. The variation of impact pressure along length is also shown upto $z_c(t)$. Figure 3.5b represents discrete points at the nodes for the plate panel of length L and shown with vertical dotted lines. Each intermediate element is of length L_i.

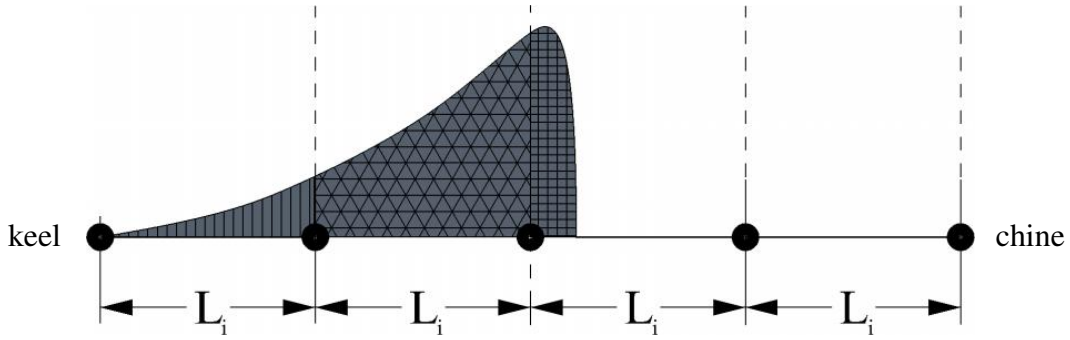

(a) Pressure zones

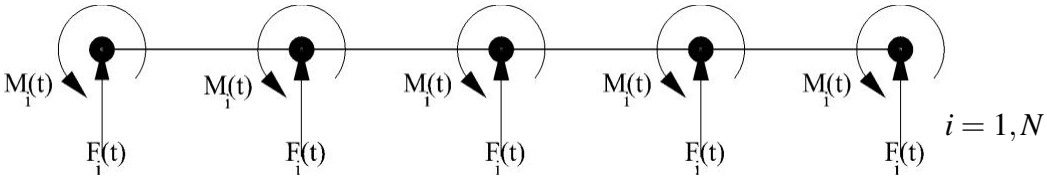

(b) Nodal Forces & Moments

Figure 3.6: Pressure to Nodal Force/Moment Evaluation: Step-2

Impact pressure function is divided at each element to create pressure zones as shown in Figure 3.6a. Each pressure zone is then integrated to calculate total force on each element. Force calculated for each element along the length of such element is then applied at the centroidal location. The total load on each element is then distributed appropriately between the bounding nodes as forces and moments.

The validation of numerical code is made using static solution and also modal expansion. The validation results are presented in Chapter 4.

CHAPTER 4
VALIDATION

Modal expansion technique is used to solve multiple degree of freedom vibration problems and its application can also be extended to ship vibration problems. A treatment to the hydroelasticity problem can be devised in a method analogous to ship vibration problems ignoring the coupling between the force and response. It is then treated in a manner similar to structural beam vibration problem in structural mechanics.

Two conditions were analyzed as discussed in the following sections to validate the code. Also, validation is made by comparing the code output with the static solution as well as the modal analysis technique. The static force is simulated as a ramp force up to peak value and thereafter it is held as constant at central node. In the modal analysis, a harmonic force is given as input at the central node.

The following particulars are used in the validation:

Material : Aluminum

Density of aluminum, ρ : 168.48 lbs/ft^3

Modulus of elasticity, E : 10,000 ksi

Bottom plate thickness, t : $1/8$ $inch$

Length : 25 $inches$

Two sets of end conditions analyzed were:

a) Pinned-Pinned (PP) Condition

b) Clamped-Clamped (CC) Condition

4.1 Static Solution

4.1.1 Pinned-Pinned beam

The static deflection of a beam of length, L with concentrated load, F at midspan and has pinned ends is given as:

$$\delta_{max} = \frac{FL^3}{48EI} \tag{4.1}$$

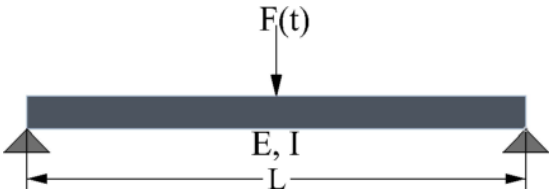

Figure 4.1: Pinned-Pinned beam

A plot between time (t) in seconds and force per unit width of plate or beam, $F(t)$ in lbs/ft is shown in Figure 4.2. The plot shows the equivalent of static force as ramped force upto certain instant of time and constant thereafter. The numerical code can thus be evaluated for accuracy in the steady state or static condition. The same input force was given for the two tested boundary conditions.

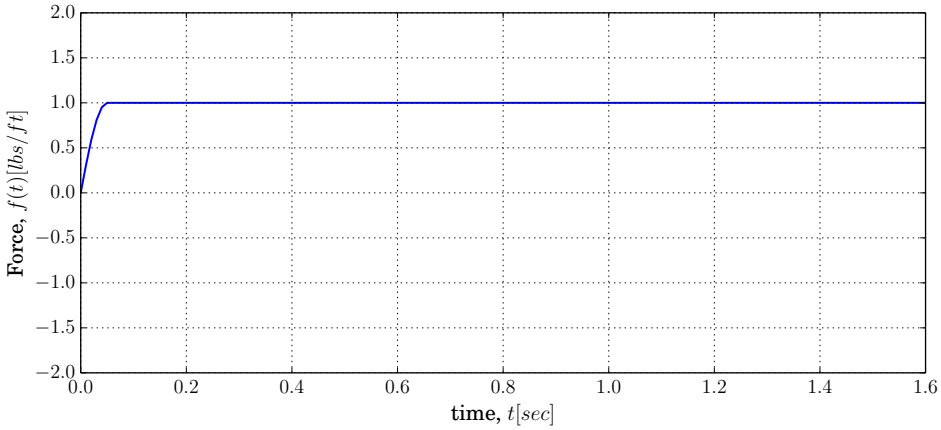

Figure 4.2: Static equivalent force

A plot between time (t) in seconds and deflection (w) in inches is shown in Figure 4.3 where the ramp-steady force as shown in Figure 4.2 is applied to the numerical code in the case of a pinned-pinned beam. This simulates a steady state input and the result show a convergence at around 0.9 seconds. A horizontal dotted line is shown to represent solution from equation (4.1). The solution matched with the calculated values in the steady state regime for both the numerical methods.

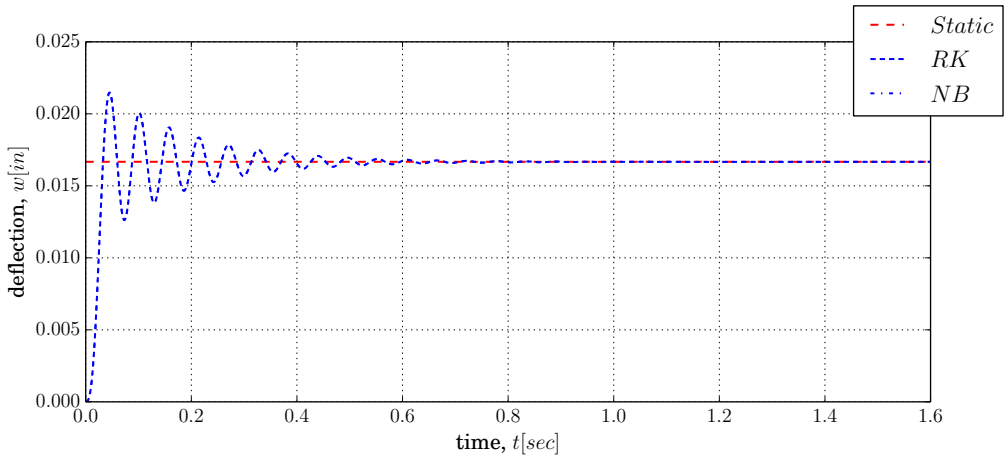

Figure 4.3: Pinned-Pinned beam - Deflection using RK4 and NB methods with 5 nodes and $\Delta t = 0.1$ *ms*

A plot between time (t) in seconds and velocity, $\dot{w}$ (ft/sec) is shown in Figure 4.4 where the numerical code is given a force input in Figure 4.2 applied on a pinned-pinned beam. This simulates a ramped steady state input and the result show a steady state convergence at around 0.9 seconds. The solution ultimately reaches to zero velocity representing a convergence to a static equilibrium in RK4 and NB methods.

A plot between time (t) in seconds and acceleration, $\ddot{w}$ (ft/sec^2) is shown in Figure 4.5 where the numerical code is given a force input in Figure 4.2 applied on a pinned-pinned beam. This simulates a ramped steady state input and the result show a steady state convergence at around 1.0 second. Solution ultimately reaches zero acceleration representing a convergence to a static equilibrium. It can also be observed that during transient phase velocity and acceleration have opposite maxima and minima as expected in a quadratic function.

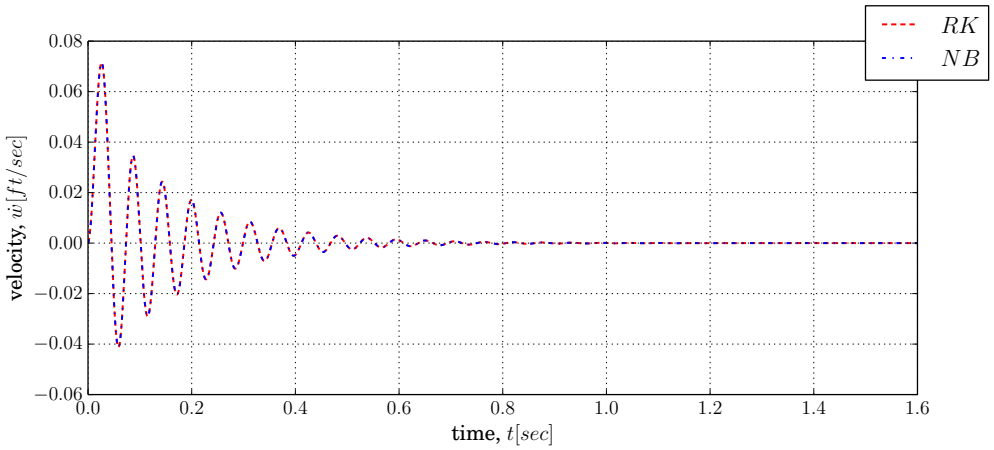

Figure 4.4: Pinned-Pinned beam - Velocity using RK4 and NB methods with 5 nodes and $\Delta t = 0.1$ *ms*

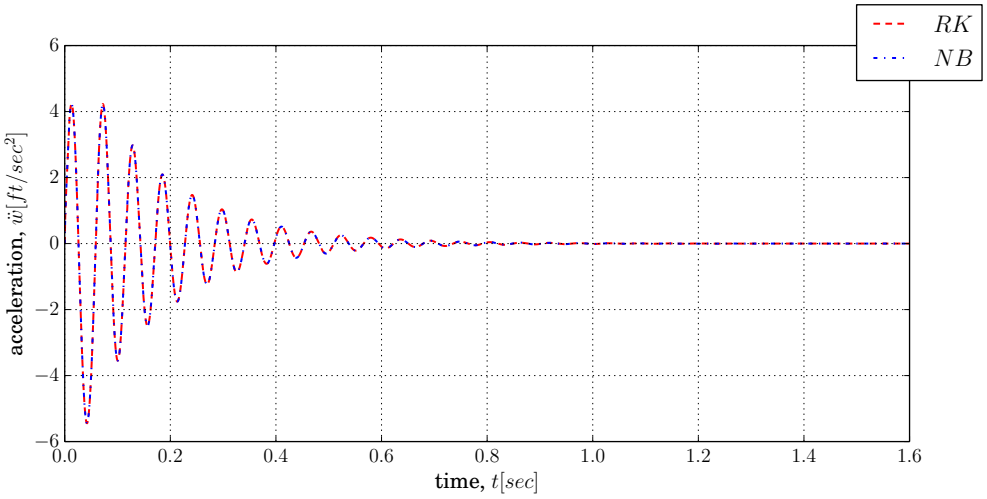

Figure 4.5: Pinned-Pinned beam - Acceleration using RK4 and NB methods with 5 nodes and $\Delta t = 0.1$ *ms*

4.1.2 Clamped-Clamped beam

The static deflection of a beam of length, L with concentrated load, F at midspan and has clamped ends is given as:

$$\delta_{max} = \frac{FL^3}{192EI} \tag{4.2}$$

Figure 4.7 deflection, Figure 4.8 velocity and figure 4.9 acceleration values are plotted against time for a clamped-clamped beam. A ramp steady state force, similar to previous section is applied on

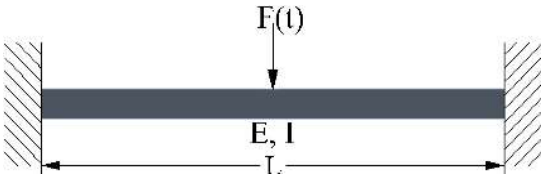

Figure 4.6: Clamped-Clamped beam

the beam. In Figure 4.7 a convergence can be seen to match a static beam deflection value in both the methods. Deflection, velocity and accelerations appear to reach a steady state regime after 0.2 seconds. Both velocity and accelerations reach a zero values when the transient phase ends. This shows that a static equilibrium had been successfully reached in both the methods.

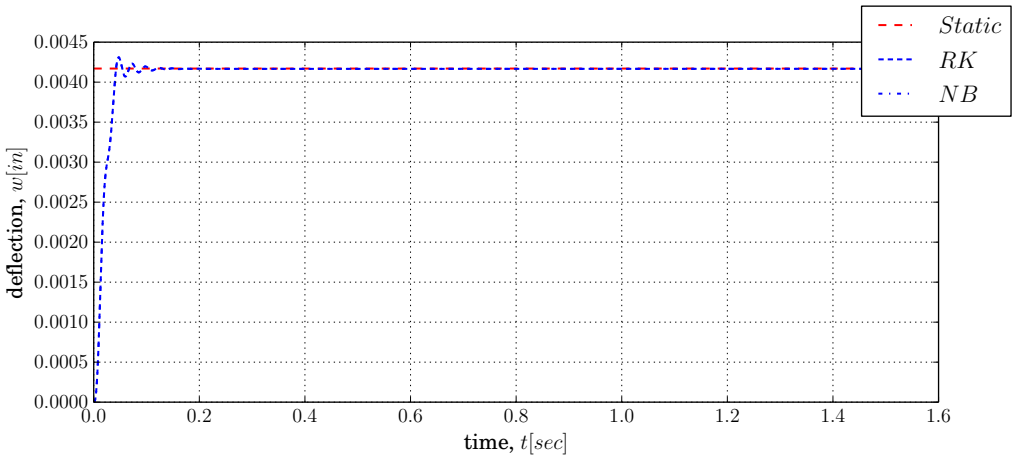

Figure 4.7: Clamped-Clamped beam - Deflection using RK4 and NB methods with 5 nodes and $\Delta t = 0.1$ *ms*

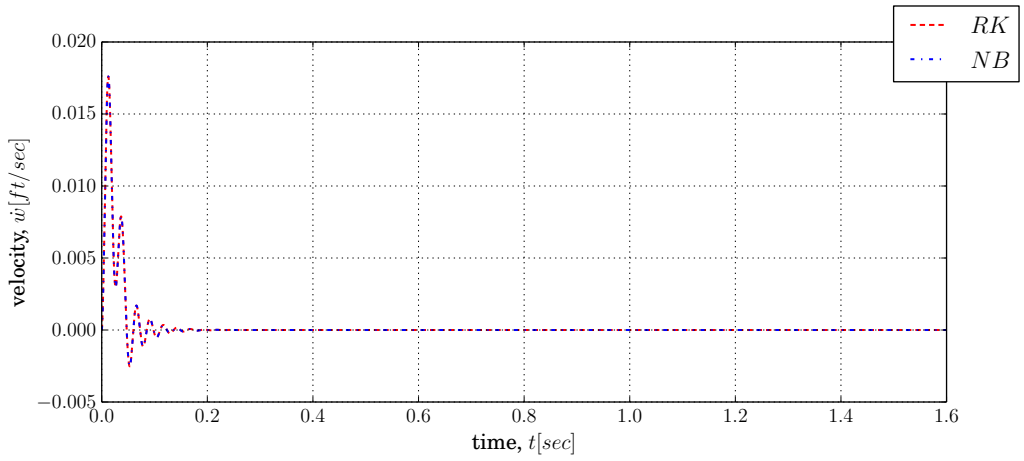

Figure 4.8: Clamped-Clamped beam - Velocity using RK4 and NB methods with 5 nodes and $\Delta t = 0.1$ *ms*

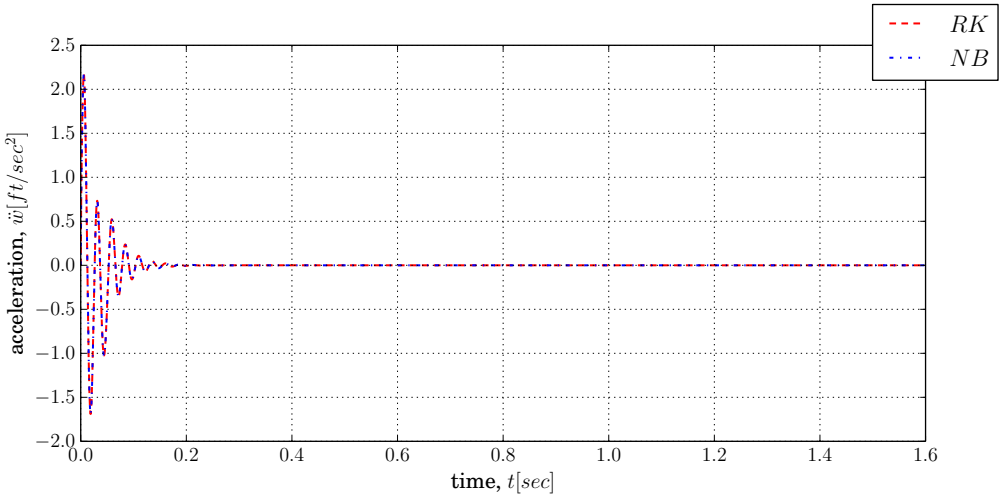

Figure 4.9: Clamped-Clamped beam - Acceleration using RK4 and NB methods with 5 nodes and $\Delta t = 0.1$ *ms*

4.2 Modal Analysis

The response of a beam under the action of harmonic force is obtained using modal analysis (MA) technique. The fundamental mode is assumed dominant, thus only bending is considered; shear deformation and rotational inertia are neglected. In effect, the beam is treated as Euler beam. The vibratory displacements are calculated as the superposition of infinite independent natural modes [2, 16].

The equation of motion for a free uniform beam with no damping is given in Equation (4.3). Additional details can be found in Vibrations section of Principles of Naval Architecture [2].

$$\frac{d^4W}{dx^4} - \kappa^4 W = 0 \tag{4.3}$$

denoting,

$$\kappa^4 = (\omega/\Omega_f)^2 - (\Omega_r/\Omega_f)^2$$

where, ω is the excitation frequency.

Characteristic flexural frequency,

$$\Omega_f = \sqrt{\frac{EI/L^3}{\mu L}}$$

Characteristic rigid-body frequency,

$$\Omega_r = \sqrt{\frac{kL}{\mu L}}$$

Here, L is the length of the beam, k is the stiffness/length, μ is the total mass/length, E is the elastic modulus, I is the moment of inertia.

The solution to the differential equation (4.3) above is

$$W(x) = C_1\, sin\ \kappa x + C_2\, cos\ \kappa x + C_3\, sinh\ \kappa x + C_4\, cosh\ \kappa x \tag{4.4}$$

4.2.1 Pinned-Pinned Condition

The deflections and moments are zero at the ends in the case of pinned-pinned beam. Non-dimensional approach has been implemented such that all length variables are non-dimensionalized

based on beam length. Thus, the boundary conditions are:

$$\begin{aligned} W(0) &= 0 & W''(0) &= 0 \\ W(1) &= 0 & W''(1) &= 0 \end{aligned} \tag{4.5}$$

Implementing Eqn. (4.5) in (4.4) yields [21]:

$$W(x) = \sin \kappa x - \left(\frac{\sin \kappa}{\sinh \kappa}\right) \sinh \kappa x \tag{4.6}$$

A plot between time (t) in seconds and force, $F(t)$ in *lbs/ft* is shown in Figure 4.10 where the force is generated to simulate a harmonic force input. This is provided so the numerical code can be evaluated for accuracy in the harmonic steady state condition. This force is applied at midspan of the beam for two different end conditions.

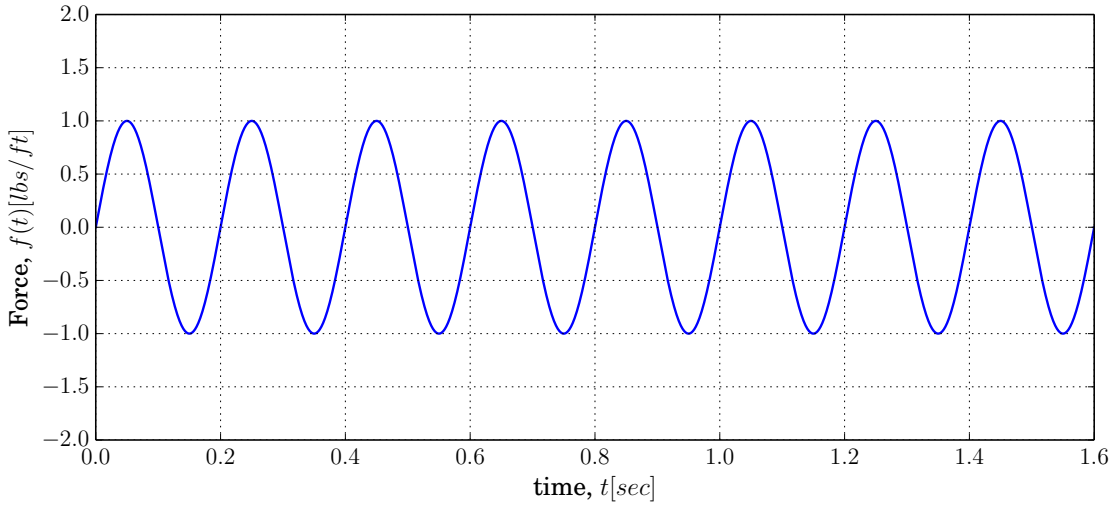

Figure 4.10: Harmonic Input force (MA)

The mode shapes for pinned-pinned beam have been shown in Figure 4.11. A deflection plot as shown in figure 4.12 shows that the beam has maximum deflection at the middle of the beam under the action of harmonic force at midspan.

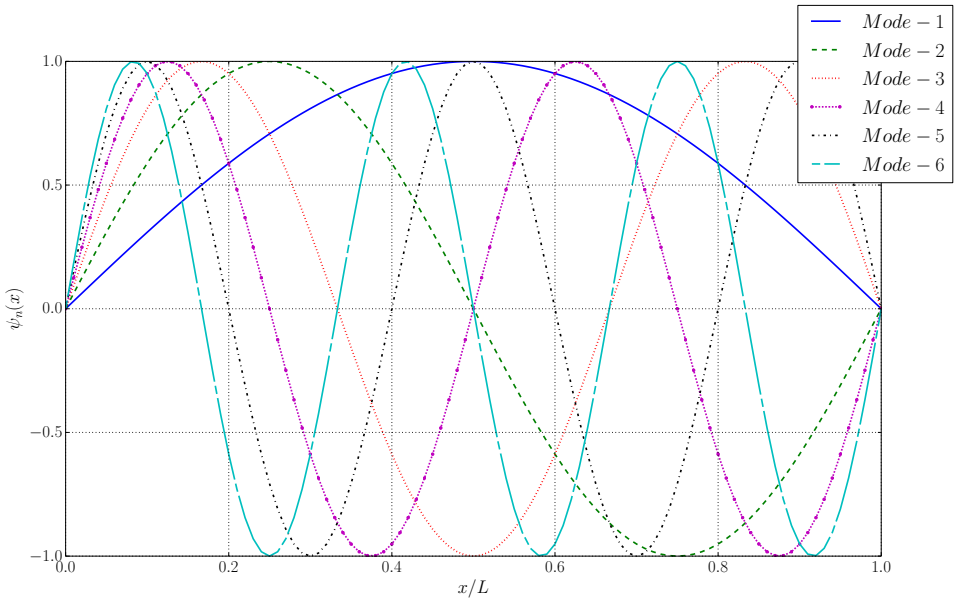

Figure 4.11: Pinned-Pinned beam - Mode shapes

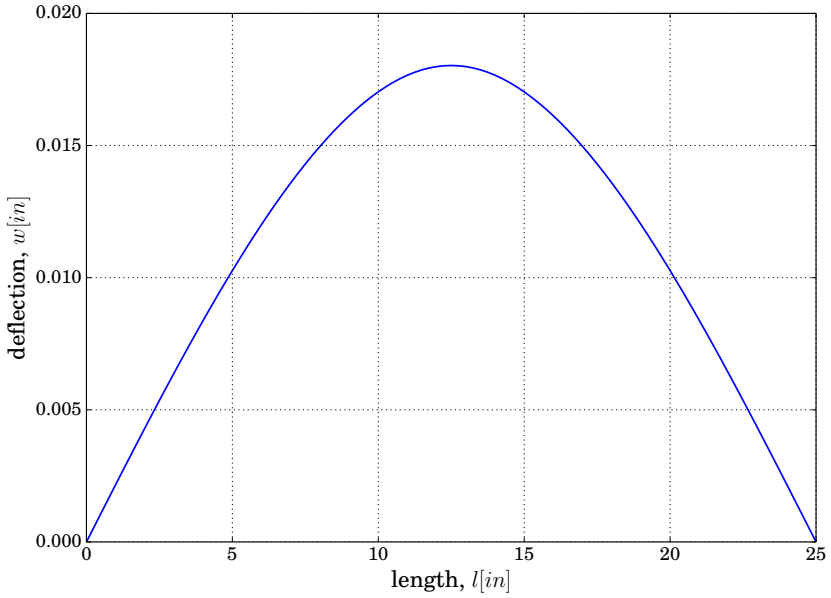

Figure 4.12: Deflection along length for a pinned-pinned beam at $t = 0.65sec$

A plot between time (t) in seconds and deflection (w) in inches is shown in Figure 4.13 where the numerical code is given an input with harmonic force as shown in Figure 4.10, which is applied on a pinned-pinned beam. This simulates a harmonic input and the result show a conver-

gence at around 0.3 seconds.

Further, as shown in figure 4.13, a comparison of deflection response using both the numerical methods is made with modal expansion for pinned-pinned beam. The results match in the steady state regime. A pinned-pinned beam shows larger variations in transient phase as the beam has less stiffness and thus subject to larger excitation. A plot between time (t) in seconds

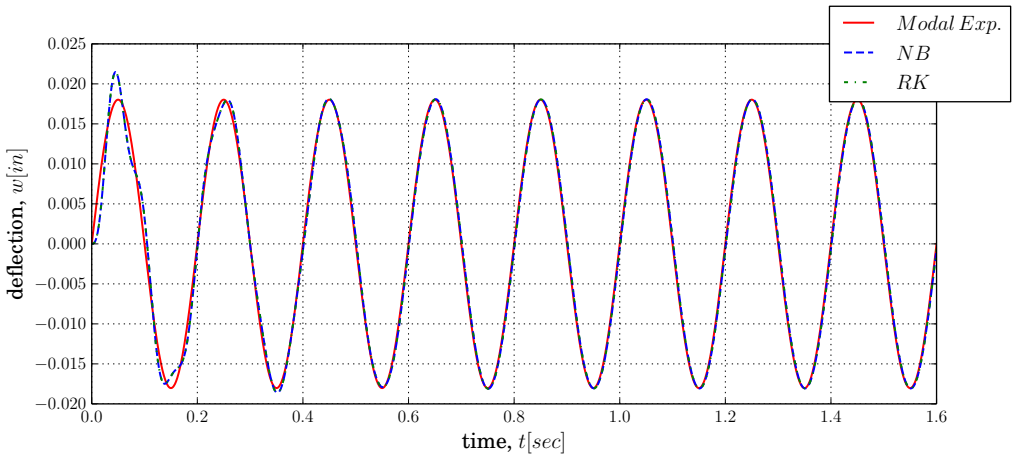

Figure 4.13: Deflection comparison between numerical methods and modal expansion for pinned-pinned beam with 5 nodes and $\Delta t = 0.1\ ms$

and velocity ($\dot{w}$) in ft/sec is shown in Figure 4.14 where the numerical code is given a force input in Figure 4.10 applied on a pinned-pinned beam. This simulates a harmonic input and the result show a convergence at around 0.5 seconds. The solution ultimately reaches harmonic response representing a convergence to steady state.

A plot between time (t) in seconds and acceleration ($\ddot{w}$) in (ft/sec^2) is shown in Figure 4.15 where the numerical code is given a force input in Figure 4.10 applied on a pinned-pinned beam. This simulates a harmonic input and the result show a convergence at around 0.9 seconds. Solution ultimately reaches harmonic response representing a convergence to steady state. It can also be observed that during transient phase velocity and acceleration have opposite maxima and minima as expected in a quadratic function.

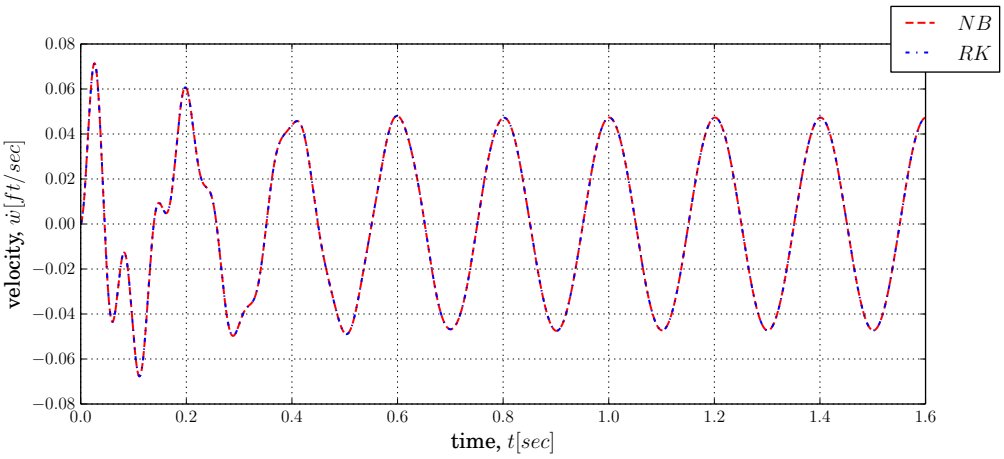

Figure 4.14: Velocity comparison plot between two numerical methods for pinned-pinned beam with 5 nodes and $\Delta t = 0.1$ *ms*

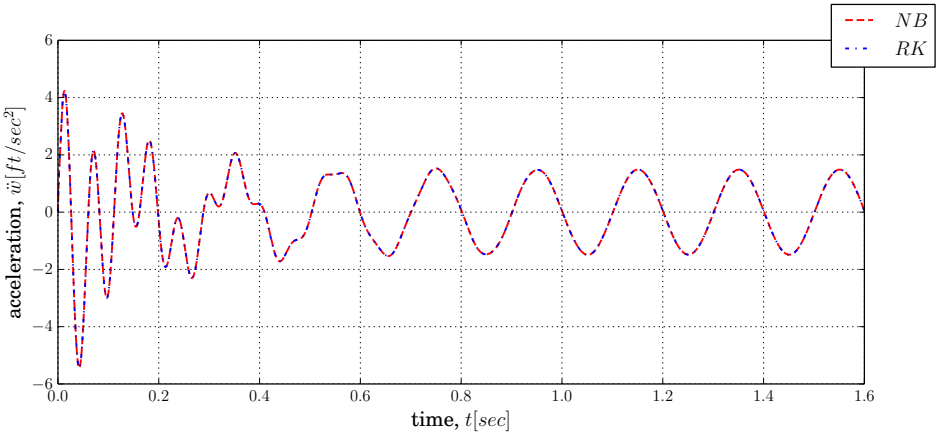

Figure 4.15: Acceleration comparison plot between two numerical methods for pinned-pinned beam with 5 nodes and $\Delta t = 0.1$ *ms*

4.2.2 Time dependency test

A plot between time (t) in seconds and deflection (w) in inches is shown using RK4 and NB method in figure 4.16 and figure 4.17 respectively. Results show a perfectly overlapping result for the time steps using both numerical methods.

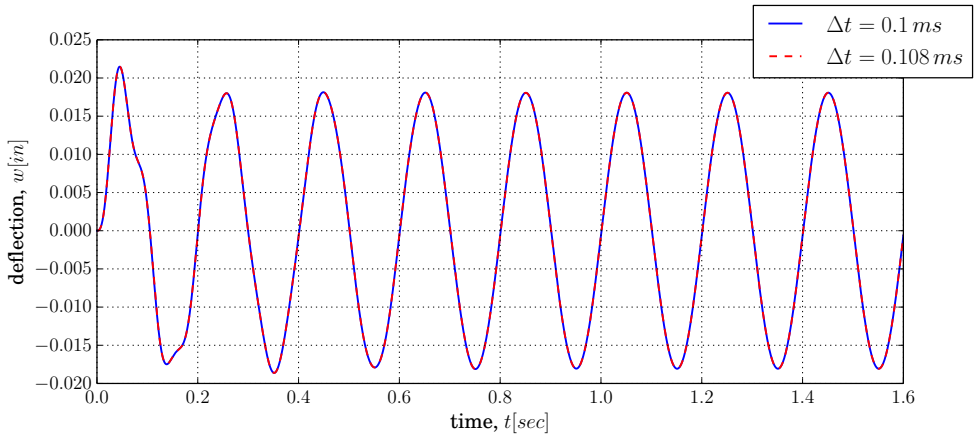

Figure 4.16: Pinned-Pinned beam time convergence test - RK4 Method with 5 nodes

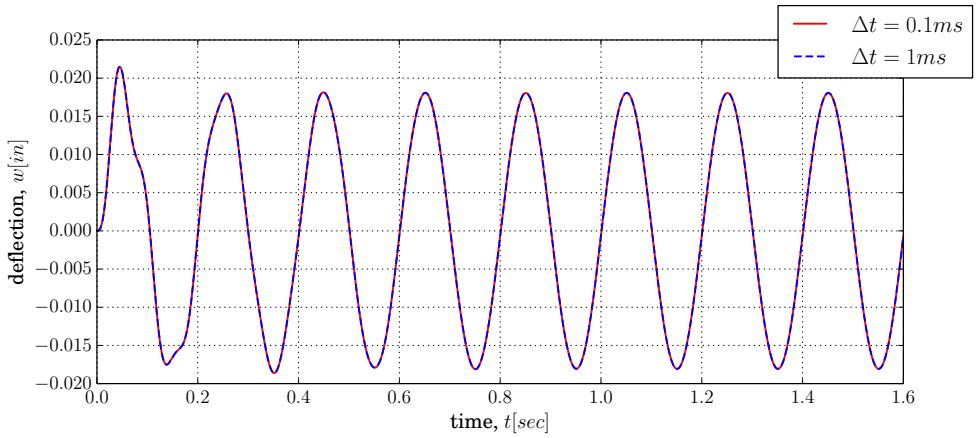

Figure 4.17: Pinned-Pinned beam time convergence test - NB Method with 5 nodes

4.2.3 Clamped-Clamped Condition

The deflection and slope doesnot exist when both the ends are clamped. Thus, the boundary conditions are:

$$\begin{aligned} W(0) &= 0 & W'(0) &= 0 \\ W(1) &= 0 & W'(1) &= 0 \end{aligned} \tag{4.7}$$

Implementing Eqn. (4.7) in (4.4) yields [21]:

$$W(x) = (cosh\ \kappa x - cos\ \kappa x) + \left(\frac{sinh\ \kappa + sin\ \kappa}{cos\ \kappa - cosh\ \kappa}\right)(sinh\ \kappa x - sin\ \kappa x) \tag{4.8}$$

The output plots for a clamped-clamped beam are shown in the following pages for the same harmonic input shown in Figure 4.10. Figure 4.18 shows mode shapes for a clamped-clamped beam which show zero slope at both ends.

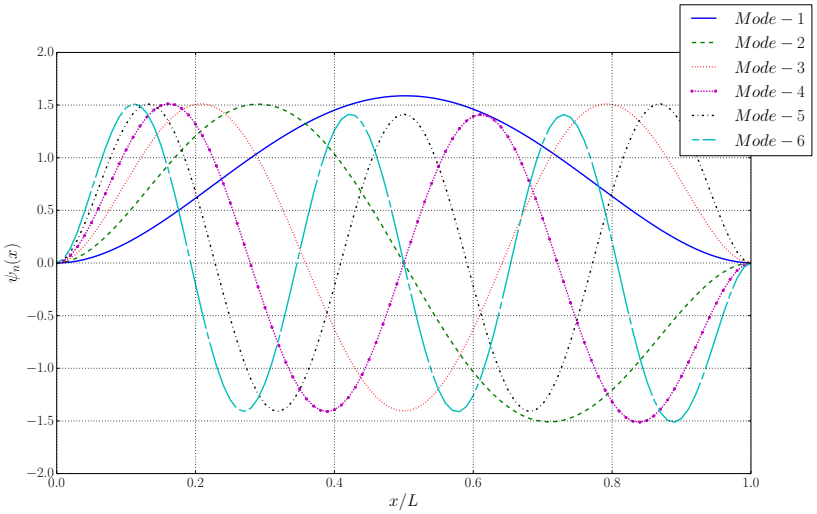

Figure 4.18: Clamped-Clamped beam - Mode shapes

A deflection plot as shown in figure 4.19 shows a beam deflection plot for clamped-clamped beam with maximum deflection at the middle of the beam when a nodal harmonic input force is applied at midspan. Ends have zero slope as expected in the case of a clamped-clamped beam.

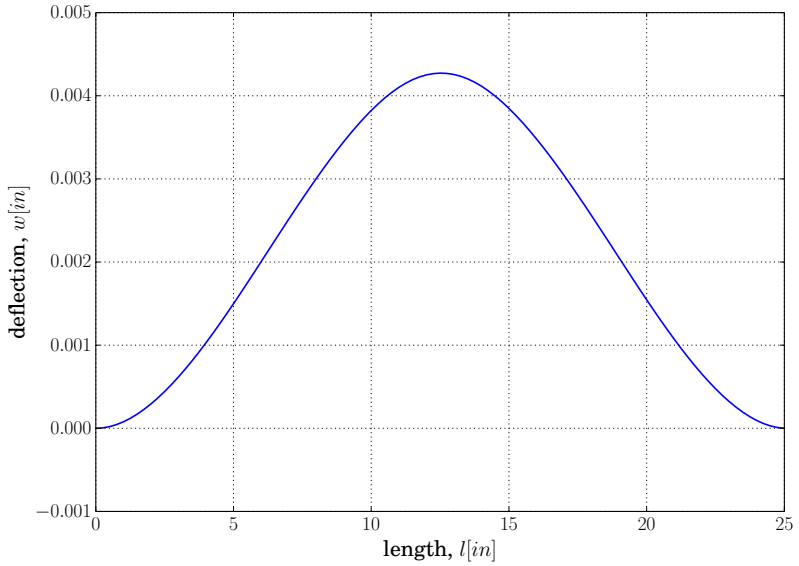

Figure 4.19: Deflection along length for a clamped-clamped beam at $t = 0.65sec$

Figure 4.20 shows a comparison of deflection response using two numerical methods with modal expansion for a clamped-clamped beam response. The results match in the steady state regime. A clamped-clamped beam shows negligible variations in transient phase in contrast to large variations in the case of pinned-pinned beam. A transient response can be seen from 0 to 0.08 seconds, and soon after a steady state response is observed.

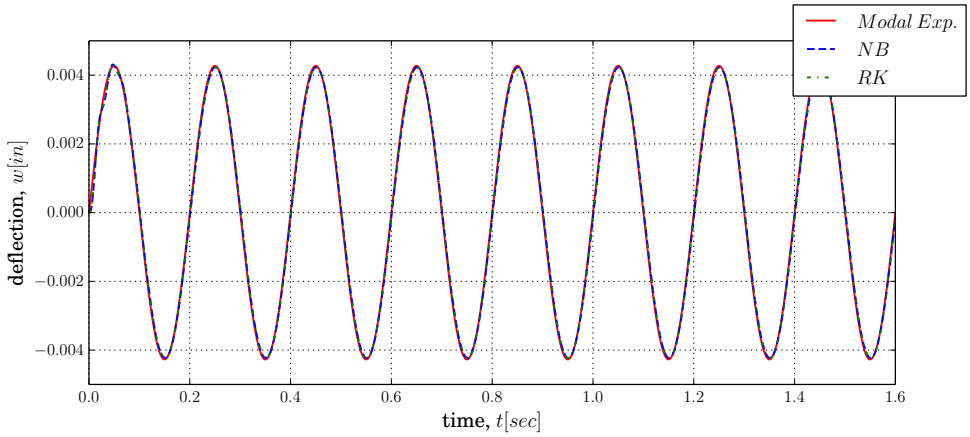

Figure 4.20: Deflection comparison between numerical methods and modal expansion for clamped-clamped beam with 5 nodes and $\Delta t = 0.1$ *ms*

A plot in figure 4.21 between time (t) in seconds and velocity ($\dot{w}$) in ft/sec has been shown for beam with a clamped-clamped end connection. A transient response can be seen from 0 to 0.11 seconds, and soon after a steady state response is observed.

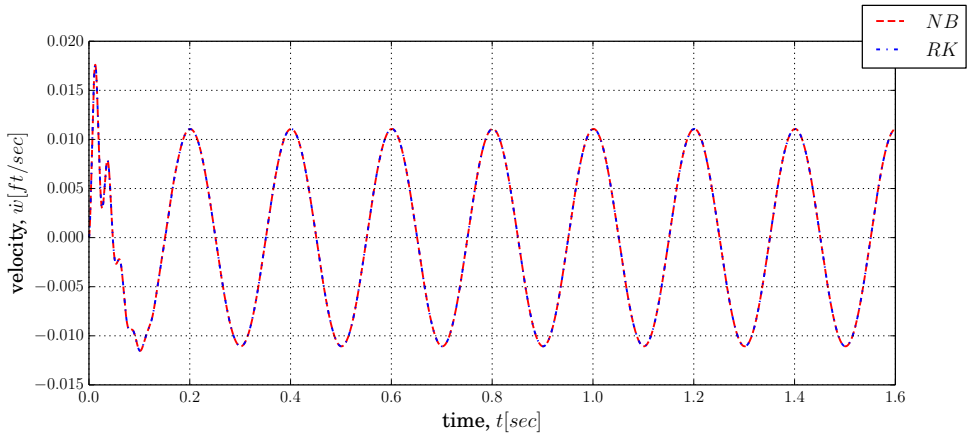

Figure 4.21: Velocity comparison plot between two numerical methods for clamped-clamped beam with 5 nodes and $\Delta t = 0.1$ *ms*

A plot in figure 4.22 between time (t) in seconds and acceleration ($\ddot{w}$) in (ft/sec^2) has been shown for beam with a clamped-clamped end connection. A transient response can be seen from 0 to 0.19 seconds, and soon after a steady state response is observed.

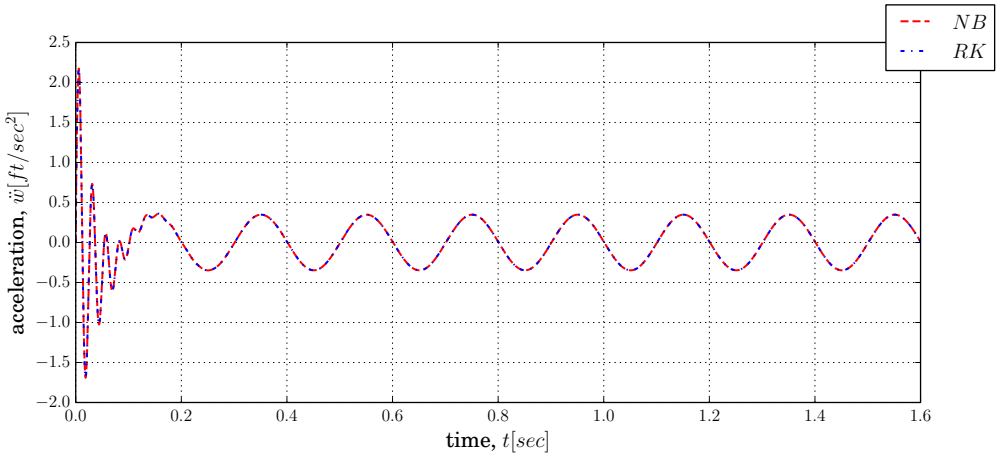

Figure 4.22: Acceleration comparison plot between two numerical methods for clamped-clamped beam with 5 nodes and $\Delta t = 0.1$ *ms*

CHAPTER 5
RESULTS OF WEDGE IMPACT ANALYSIS

The dimensions of the wedge section considered in the present analysis is discussed. The time convergence test for the impact force and the response is presented in this chapter. The results of the time convergence test are also presented. In addition, the deflection is compared for different number of nodes. A comparison between the two different boundary conditions (PP & CC) with an impact velocity of 9.51 ft/sec is also presented. The deflection for three different bottom plate thicknesses using both the boundary conditions is also compared.

5.1 Wedge Model Particulars

A prismatic hull is considered in the present analysis. The following are the hull particulars:

- Material : Aluminum
- Modulus of elasticity : 10,000 *ksi*
- Structural damping factor : $tan\delta = 0.001$
- Wedge weight : 79.02 lb/ft
- Bottom plate thickness: $1/4$ *inch*
- Maximum Beam : 47.244 *inches*
- Maximum Depth : 21 *inches*
- Deadrise angle : 20°

The code was tested for stability by changing the number of elements and time steps. A numerical breakdown occurred as the number of elements are increased in case of RK4 method. This can be attributed to an increased stiffness of the system, which could lead to the failure of the Runge-Kutta scheme. A four element *i.e., five noded* beam is considered a limiting case using RK4 method for $\Delta t = 0.1$ *ms*. This is dependent on the time step size. However, there is no such case for NB method because the method is unconditionally stable. All the results in this section are presented

using NB method for 17 nodes (16 elements) where the convergence was achieved. The impact hydrodynamic force is resolved into force/moment at each node using the method explained in Chapter 3. The maximum values of deflection, velocity and acceleration are presented in this chapter.

5.2 Time Convergence test

The time convergence test was conducted to analyze the stability of the dynamic system. The stability of the system is checked for different time steps at impact velocity of $V = 9.51 ft/s$. The results are presented in the following sections. The excitation at three different time steps at one (central node 9) of the 17 nodes is shown in figure 5.1. The corresponding deflection plot is also shown in figure 5.2. Also, the plot of added mass is shown in figure 5.3.

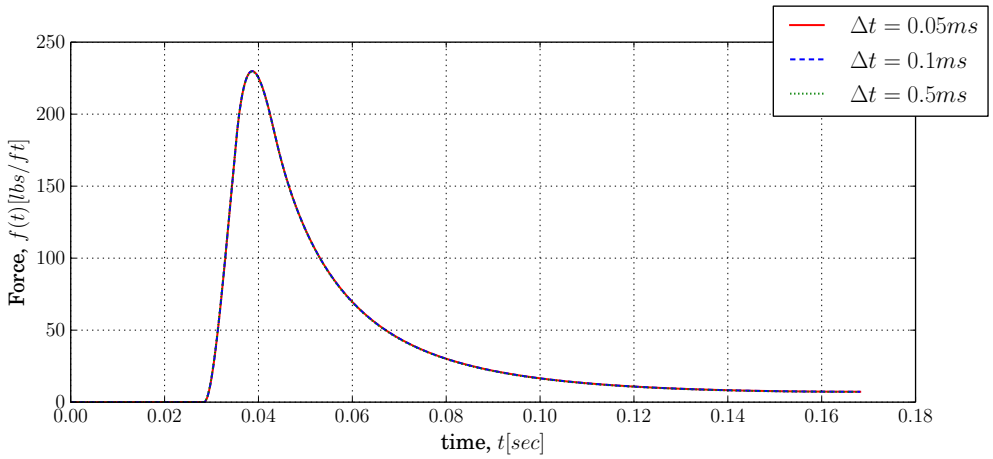

Figure 5.1: Comparison of impact force at central node at different time steps with impact velocity, $V = 9.51 ft/s$ for 17 noded model

The results indicated that the stability can be achieved in the system even with the time step, $t = 0.5ms$. It was also observed that the system transient phase cannot be captured for any value higher than the time step, $t = 0.1ms$ using RK4 method. However, for improved accuracy in the solution, smaller time steps are to be selected in case of NB method. The excitation force, deflection and added mass values overlapped each other respectively at all the time events.

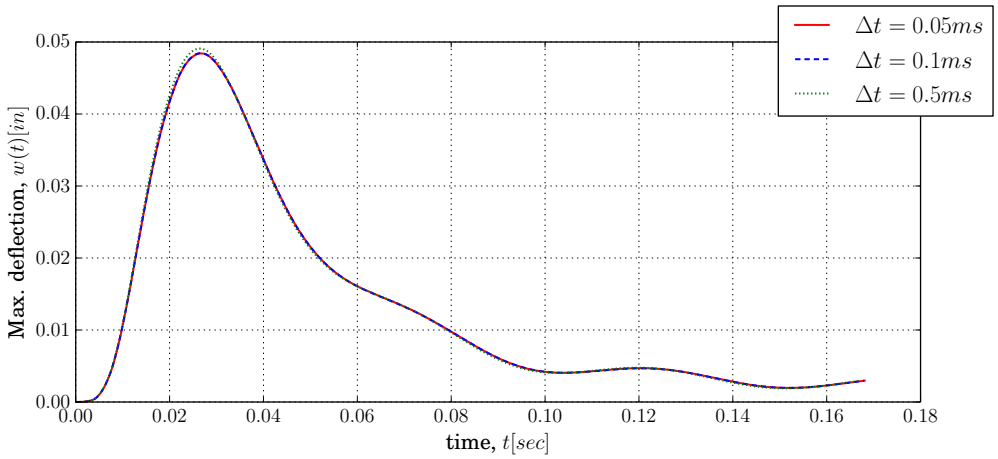

Figure 5.2: Comparison of maximum deflection for clamped-clamped beam at different time steps with impact velocity, $V = 9.51 ft/s$ for 17 noded model

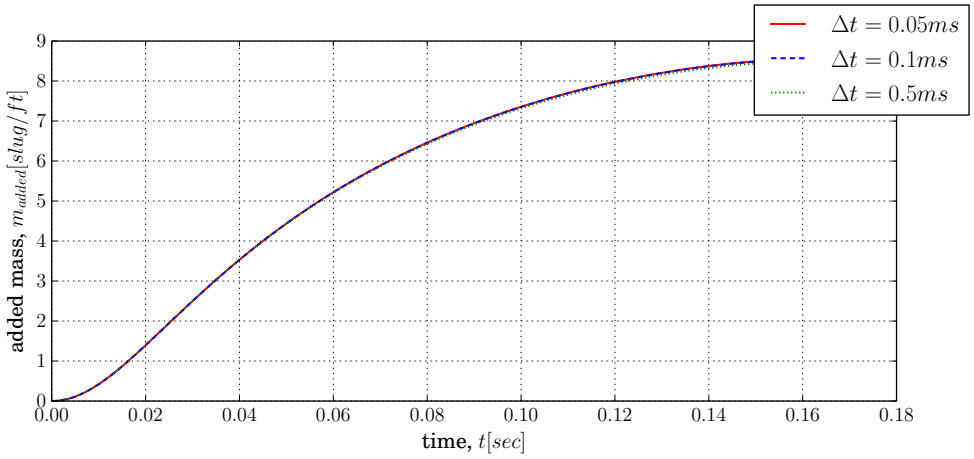

Figure 5.3: Comparison of added mass at different time steps with impact velocity, $V = 9.51 ft/s$ for 17 noded model

5.3 Node variation test

The beam response is also evaluated for different number of nodes in order to check the stability of the system. The results are presented in the following pages. An impact velocity of $9.51 ft/s$ is considered in the present analysis. The total excitation force and a typical excitation force at each node using five nodes is shown in the figure 5.4. The peak forces are observed for very short duration. The peak excitation at the node is at the instant when the node was wet.

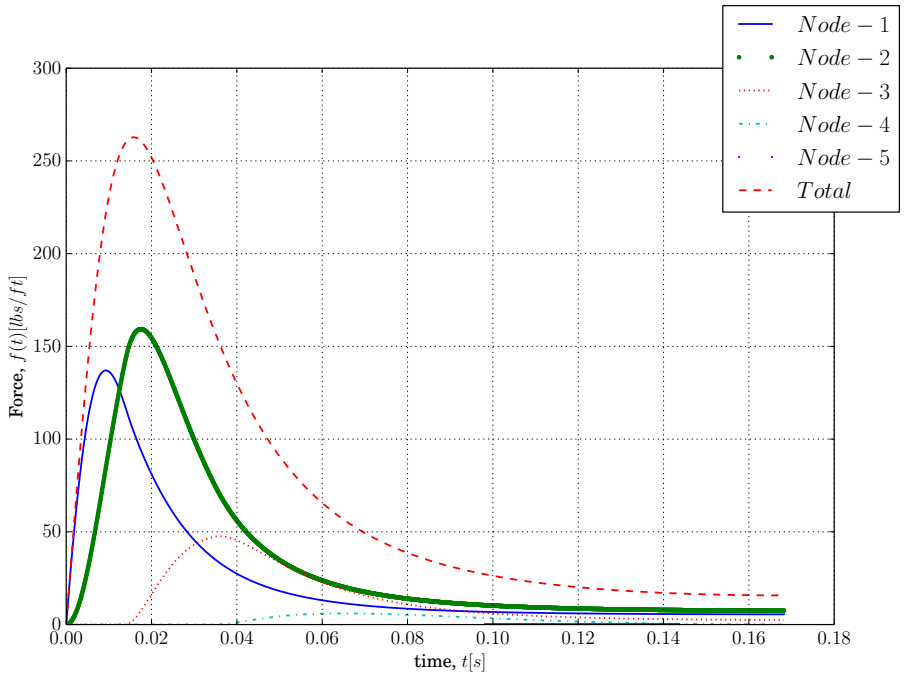

Figure 5.4: Typical plot of impact force at each node with impact velocity, $V = 9.51 ft/s$ for 5 noded model

Figure 5.5 shows the comparison of maximum deflection for a clamped-clamped beam. It is observed that the increase in the number of nodes increased the accuracy in NB method. The maximum deflection is observed as 0.048 inches at t = 0.028 sec. It is also observed that system is converged with 17 nodes.

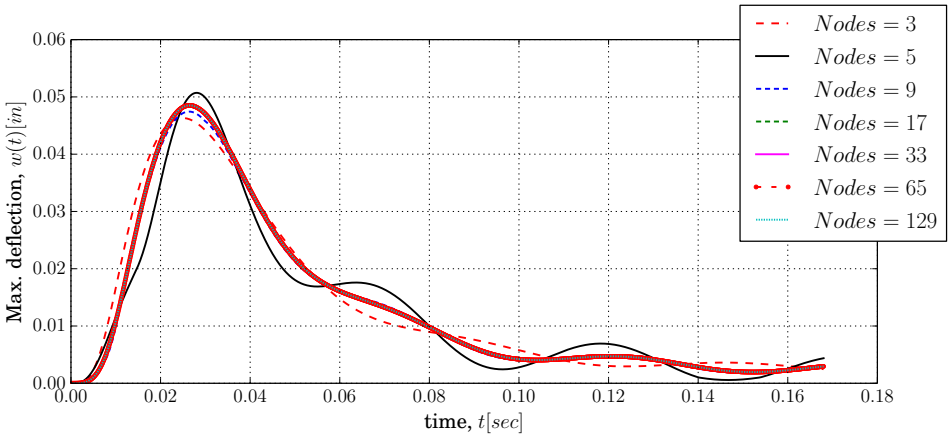

Figure 5.5: Comparison of maximum deflection at impact velocity, $V = 9.51 ft/s$ using different nodes for a clamped-clamped beam

Figure 5.6 shows the comparison of maximum deflection for a pinned-pinned beam. It is observed that the increase in the number of nodes increased the accuracy in NB method. The maximum deflection is observed as 0.40 inches at t = 0.028 sec. It is also observed that system is converged with 17 nodes. The deflection is also significantly high when compared to clamped ends.

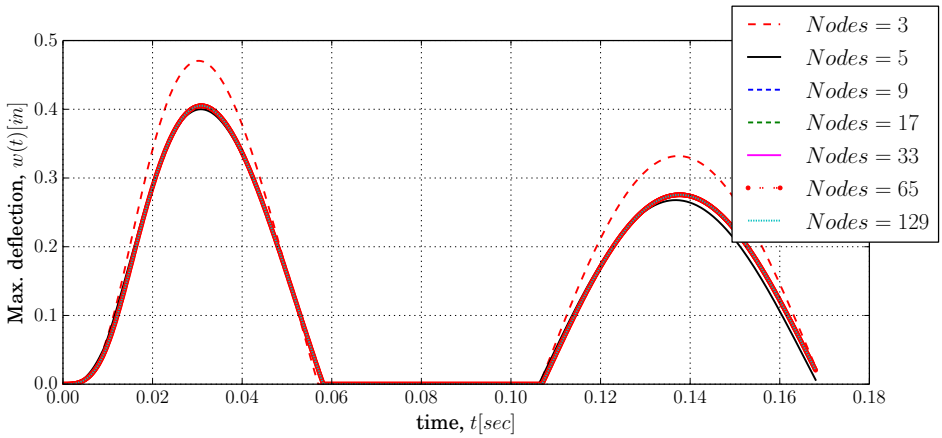

Figure 5.6: Comparison of maximum deflection at impact velocity, $V = 9.51 ft/s$ using different nodes for a pinned-pinned beam

The immersion of wedge at each step and the corresponding deflection of the bottom panel with both ends pinned and clamped are shown in Figure 5.7-5.13. In all the conditions, the maximum deflection is high with pinned ends when compared to clamped ends. The maximum deflection is 0.40 *inches* and observed at $t = 0.028s$ in case of pinned ends. Whereas, the maximum deflection is 0.048 *inches* at $t = 0.028s$ with clamped ends.

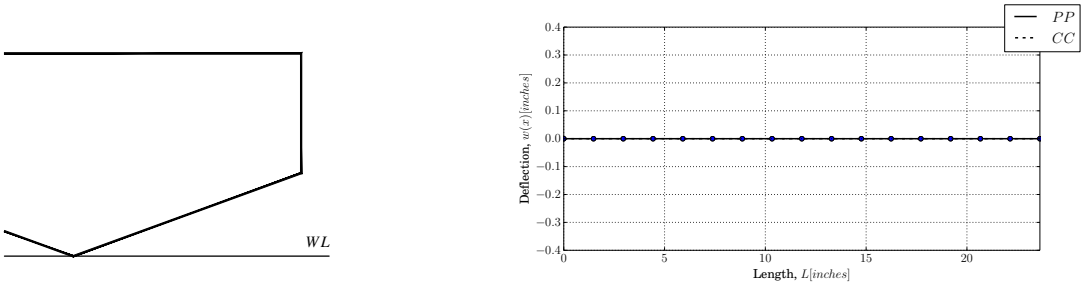

(a) Wedge

(b) Initial condition

Figure 5.7: Wedge and bottom panel in initial condition at $t = 0s$ with 17 nodes

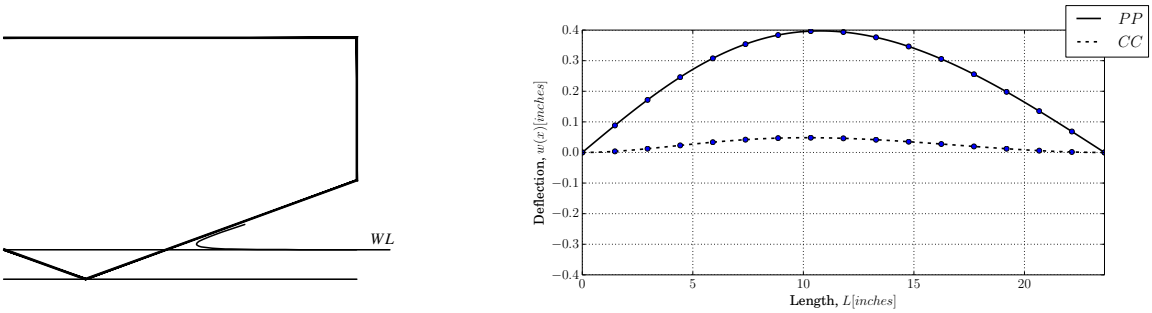

(a) Wedge (b) Deflection

Figure 5.8: Wedge immersion and deflection at $t = 0.028\,s$ with 17 nodes

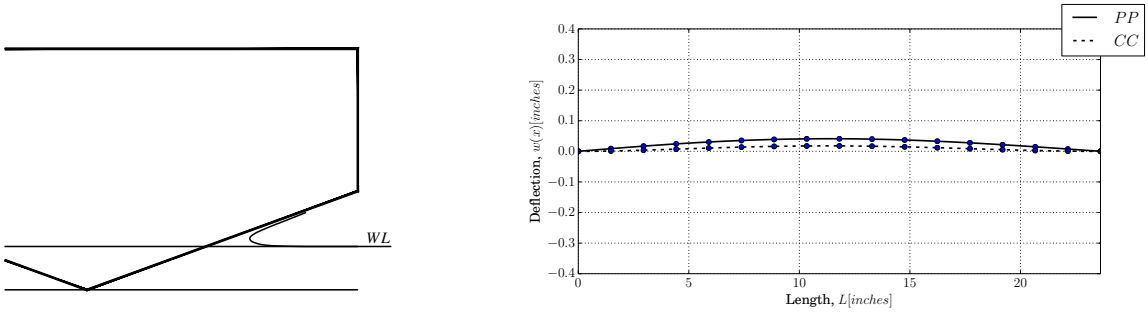

(a) Wedge (b) Deflection

Figure 5.9: Wedge immersion and deflection at $t = 0.056\,s$ with 17 nodes

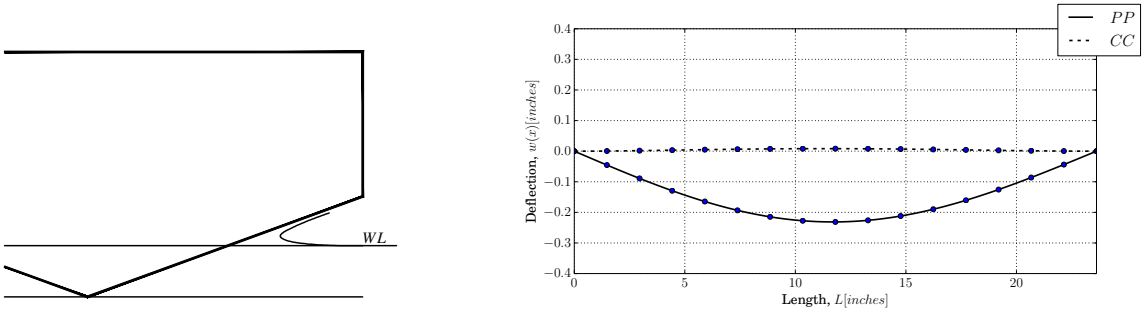

(a) Wedge (b) Deflection

Figure 5.10: Wedge immersion and deflection at $t = 0.084\,s$ with 17 nodes

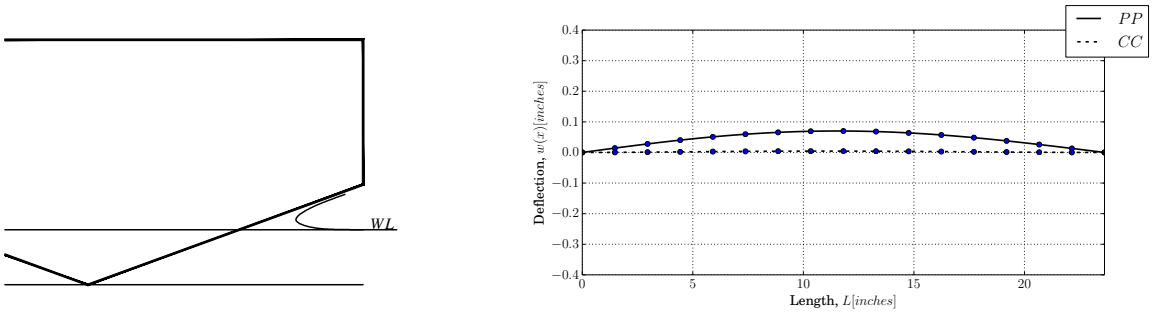

(a) Wedge (b) Deflection

Figure 5.11: Wedge immersion and deflection at $t = 0.112\,s$ with 17 nodes

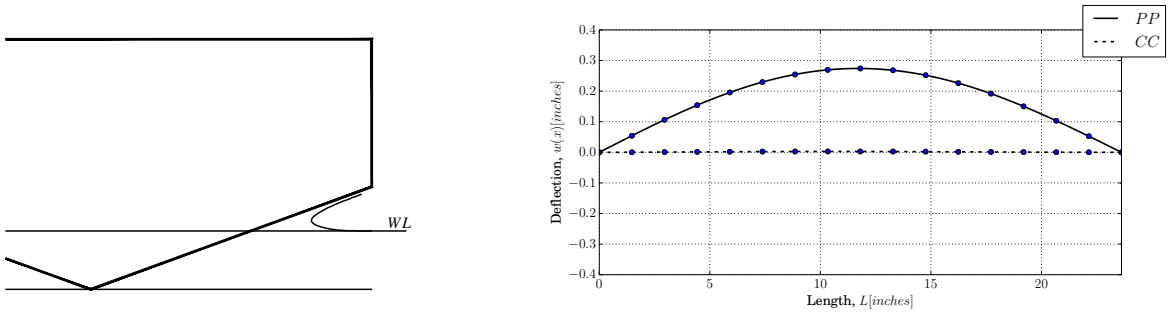

(a) Wedge (b) Deflection

Figure 5.12: Wedge immersion and deflection at $t = 0.140\,s$ with 17 nodes

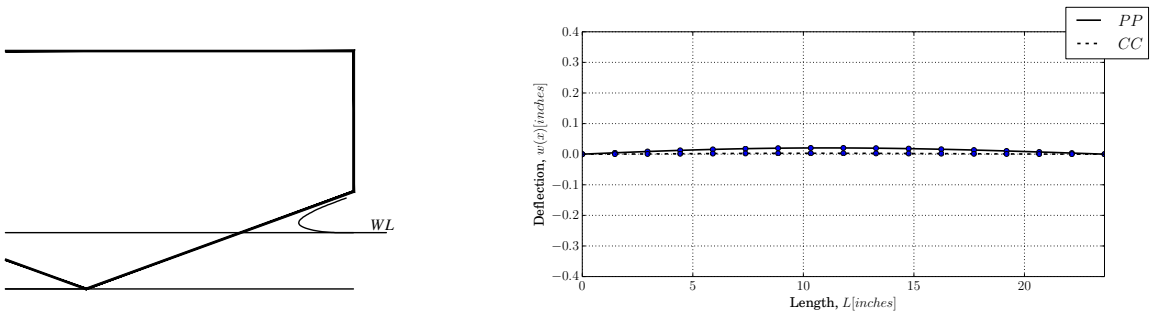

(a) Wedge (b) Deflection

Figure 5.13: Wedge immersion and deflection at $t = 0.168\,s$ with 17 nodes

5.4 Boundary Condition variation test

In boundary condition variation tests, two different boundary conditions are tested namely pinned end (PP) and clamped (CC) at both ends. The boundary condition test was conducted for 1/4" thick plate using an impact velocity of 9.51 ft/sec and 17 nodes. The boundary condition test was conducted with time step, $t = 0.1ms$. The results of the test are shown in the following pages.

Figure 5.14 shows a quantitative as well as qualitative comparison of maximum deflection between the two boundary conditions at impact speed of $V = 9.51ft/s$. It is clear that the maximum deflections are significantly low in clamped condition when compared to pinned ends. This is due to inherent rigidity at the ends of the beam when the ends are clamped. Thus, appropriate end treatments are essential.

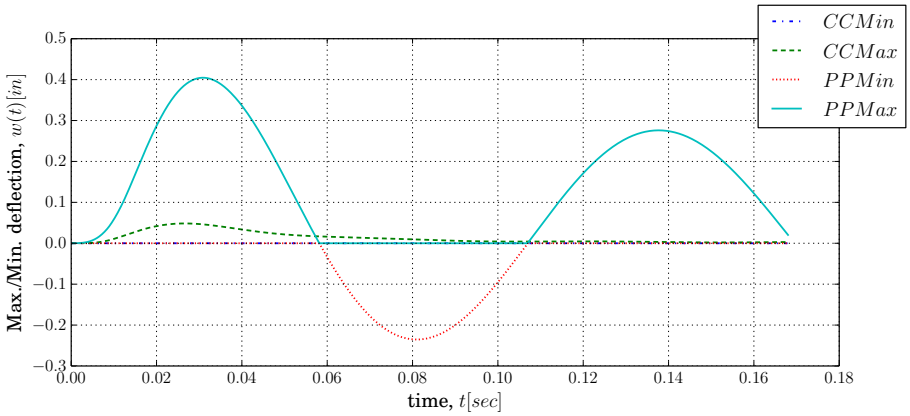

Figure 5.14: Comparison of maximum/minimum deflection between two different end conditions at impact velocity, $V = 9.51ft/s$ for a 17 noded model

5.5 Thickness variation test

The beam response is also evaluated for three different plate thicknesses. The comparison plots are shown in the following pages. An impact velocity of $9.51ft/s$ with 17 nodes is considered in the present analysis.

Figure 5.15 indicates that deflection is significantly high for smaller thickness. This is because the plate is essentially soft. The increase in thickness increases the stiffness and thus yields low maximum deflection in the total system in the case of pinned ends. Figure 5.16 shows

the minimum deflection plot with pinned ends. The absolute minimum deflection magnitude of the system is slightly lower than the maximum deflection as expected because of structural damping in the system.

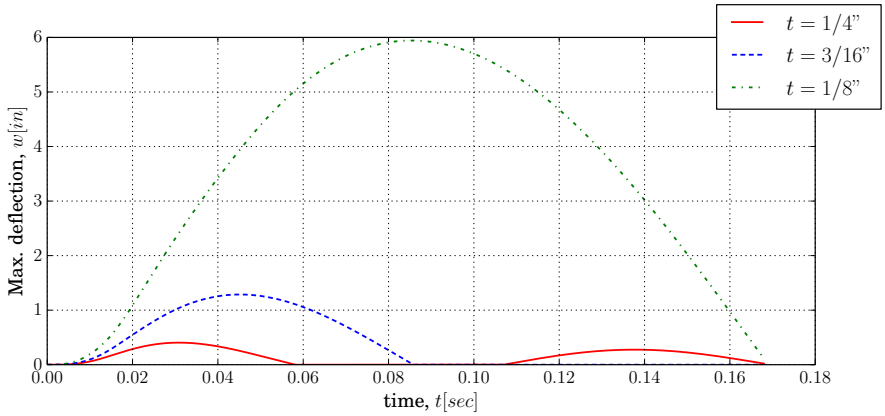

Figure 5.15: Comparison of maximum deflection with impact velocity, $V = 9.51 ft/s$ using 17 nodes for different thicknesses for a pinned-pinned condition

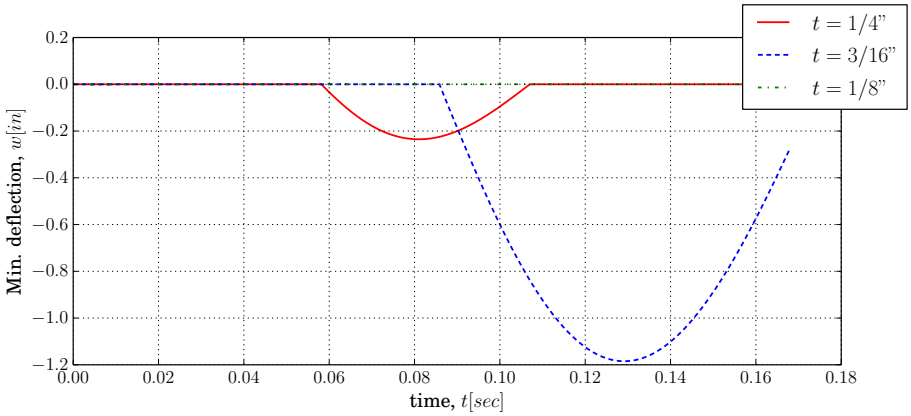

Figure 5.16: Comparison of minimum deflection with impact velocity, $V = 9.51 ft/s$ using 17 nodes for different thicknesses for a pinned-pinned condition

Figure 5.17 shows the comparison of maximum deflection for different thicknesses for beam with clamped ends. The plot indicates that deflection is high for smaller thickness similar to the case of pinned ends. The beam has zero deflection at two time instants for 1/8” thick plate when ends are clamped. In contrast to this, zero deflection was observed when the plate is 3/16” and at single instant in case of pinned ends. In effect, the zero deflection points increased with thickness in case of pinned ends and decreased in case of clamped ends.

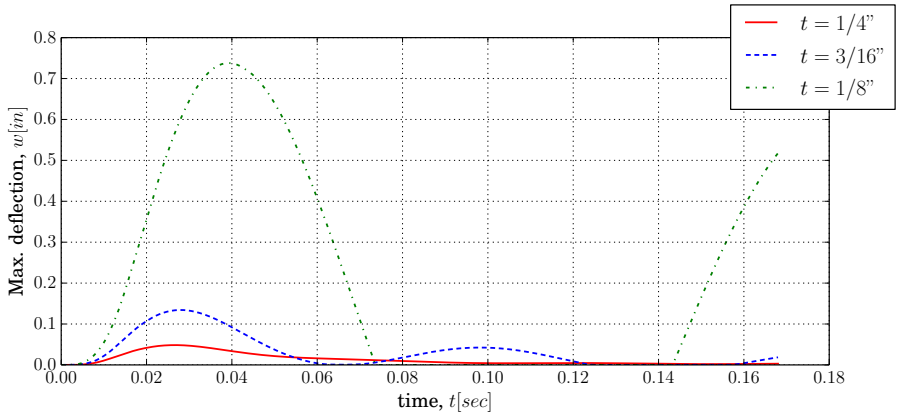

Figure 5.17: Comparison of maximum deflection with impact velocity, $V = 9.51 ft/s$ using 17 nodes for different thicknesses for a clamped-clamped condition

Figure 5.18 also shows the minimum deflection plot with clamped ends similar to Figure 5.16. The absolute minimum deflection magnitude of the system is slightly lower than the maximum as expected because of damping in the system. Also the system underwent slightly higher damping when compared to the system with pinned ends.

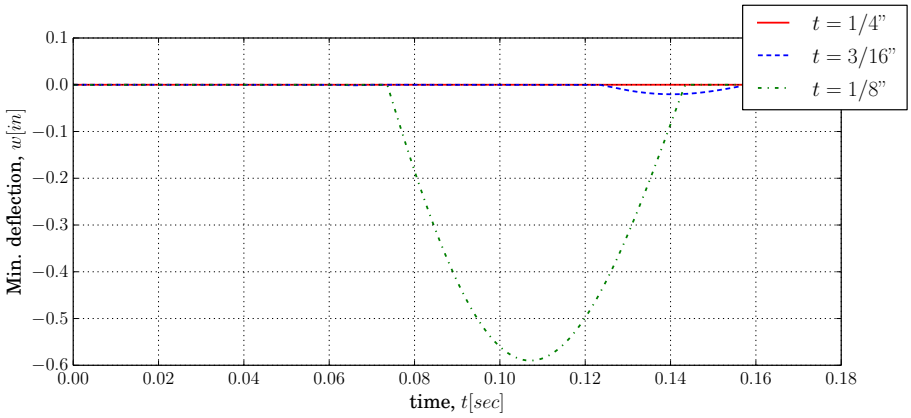

Figure 5.18: Comparison of minimum deflection with impact velocity, $V = 9.51 ft/s$ using 17 nodes for different thicknesses for a clamped-clamped condition

CHAPTER 6
CONCLUSIONS

A code has been formulated in FORTRAN to predict the response under impact force. The fourth order Runge-Kutta (RK4) method and Newmark-β (NB) methods have been successfully applied to solve the dynamic impact problems. A time dependency test has also been conducted to check the possibility of becoming a stiff equation with the input variables to avoid breakdown of the numerical scheme. The reasons for numerical breakdown was ascertained as smaller time steps and the minimum timestep value as 0.1 ms. Also, a finite increase in the number of elements can lead to a stiff equation and a possible numerical breakdown. Thus, number of elements and time step (Δt) are to be carefully considered for RK4 method. The selection of time step will improve the accuracy of the solution in case of Newmark method.

The accuracy of the code has been verified against a traditional simple static solution. Also, the code has been validated using the modal expansion technique. The static solution was recovered and also steady state was obtained for two different boundary conditions *viz.,* pinned-pinned and clamped-clamped using both the numerical schemes.

In addition, a hydrodynamic pressure is given as input to the code. The nodal forces are calculated and applied at each node to obtain the response. Time dependency has been verified and observed the minimum timestep value as 0.1 ms with 4 elements along the length are essential for RK4 method. It was also observed that proper selection of time step and appropriate selection of the number of elements is essential for RK4 method. A discussion is also made in the results section about the responses obtained for the given impact force. The deflection response for three different plate thicknesses was evaluated and compared. In addition, two different boundary conditions were tested at impact velocity of 9.51 ft/sec and also compared. The deflection in case of pinned connection was high when compared to clamped condition.

In conclusion, a numerical tool is at dispense to calculate the response under an impact force. The predicted peak magnitudes can be used as a basis for the selection of the instruments (*strain gage, velocity sensors etc.*) used in the tow tank testing. Numerical breakdown may occur unless judicious selection of time step is not made for RK4 method. The timestep and increase in the node quantity improved the accuracy of the solution. The numerical code can be used to analyze the structural strength of panels along with two dimensional simplification with reasonable accuracy to ascertain the limit stress under impact loads. An impact force is significantly high for very short duration and can overstress the panel beyond its safe limit. A pinned-pinned although conservative overpredicts the structural response when compared to a clamped-clamped connection. Thus, a proper selection of boundary condition is necessary for a more practical and feasible solution. Also the structural response predicted is large because of high aspect ratio assumption of the panel. In effect, an appropriate selection of aspect ratio is also essential.

6.1 Limitations

The limitations of the numerical code are two-dimensionality, limited number of elements required to avoid numerical breakdown for RK4 method, the total time steps should always be a multiple of 2. Also, very small time step has to be chosen to avoid numerical breakdown of RK4 method. Proper selection of node quantity is essential in case of Newmark method for a more accurate solution.

6.2 Future Work

Without loss of generality, the present work can be extended to calculate the total 3D plate panel response. The present work assumed one way coupling between the force and the response. Also, the accurate prediction can be made if the force system and response can be coupled and integrated into single code. The code if extended to full plate panel can be used as a design basis for the hull structural design by integrating it into the design spiral. An experimental work is needed to fully validate the results of the numerical code.

BIBLIOGRAPHY

[1] R. E. D. Bishop and W. G. Price. *Hydroelasticity of ships*. Cambridge University Press, 1979.

[2] Edward V. Lewis (Editor). *Principles of Naval Architecture*. The Society of Naval Architects and Marine Engineers, 1988.

[3] Volker Bertram. *Practical Ship Hydrodynamics*. Butterworth-Heinemann, 2000.

[4] Th. von Kármán. The impact on seaplane floats during landing. Technical Report No. 321, National Advisory Committee for Aeronautics, 1929.

[5] Herbert Wagner. Phenomena associated with impacts and sliding on liquid surfaces. Technical Report No. 4, Vol. 12, Zeitschrift fur angewandte Mathematik und Mechanik, August 1932.

[6] William S. Vorus. A flat cylinder theory for vessel impact and steady planing resistance. *Journal of Ship Research*, 40(No. 2), June 1996.

[7] Odd M. Faltinsen. Water entry of a wedge by hydroelastic orthotropic plate theory. *Journal of Ship Research*, 43(No. 3):180–193, September 1999.

[8] A. Korobkin , R. Guéret, and Š. Malenica. Hydroelastic coupling of beam finite element model with Wagner theory of water impact. *Journal of Fluids and Structures*, 22, 2006.

[9] Dominic J. Piro and Kevin J. Maki. Hydroelastic wedge entry and exit. In 11^{th} *International Conference on Fast Sea Transportation*, pages 653–660. American Society of Naval Engineers, 2011.

[10] Dominic J. Piro. *A Hydroelastic Method for the Analysis of Global Ship Response Due to Slamming Events*. PhD thesis, University of Michigan, 2013.

[11] Nabanita Datta. *Hydroelastic Response of Marine Structures to Impact-Induced Vibrations*. PhD thesis, University of Michigan, 2010.

[12] Christine Ikeda. Slamming load effects on the bottom of high-speed aluminum planing craft. In 13^{th} *International Conference on Fast Sea Transportation*. The Society of Naval Architects and Marine Engineers, 2015.

[13] Christine Ikeda. Deflections on the bottom of a wedge-shaped hull due to slamming loads. In *World Maritime Technology Conference*. The Society of Naval Architects and Marine Engineers, 2015.

[14] Jian Lv and Joachim L. Grenestedt. Some analytical results for the initial phase of bottom slamming. *Marine Structures*, 34:88–104, 2013.

[15] A. Korobkin and R. Guéret, and Š. Malenica. Validation of high fidelity CFD/FE FSI for full-scale high-speed planing hull with composite bottom panels slamming. In 13^{th} *International Conference on Fast Sea Transportation*. The Society of Naval Architects and Marine Engineers, 2015.

[16] Brandon M. Taravella. NAME 6121, Lecture Notes. *University of New Orleans*, Fall 2014.

[17] Carolina Hermida-Merino, Martin Perez-Rodriguez, Manuel M. Pineiro, and Maria Jose Pastoriza-Gallego. Evidence of viscoplastic behavior of exfoliated graphite nanofluids. *Soft Matter*, 12:2264–2275, 2016.

[18] William T. Thomson. *Theory of Vibration with Applications*. Prentice-Hall, Inc., 1981.

[19] M. Géradin and D. Rixen. *Mechanical Vibrations: Theory and Applications to Structural Dynamics*. Wiley, John & Sons, Incorporated, 1997.

[20] Peter J. Olver. Numerical solution of ordinary differential equations. *Numerical Analysis Lecture Notes*, 2008.

[21] Cyril M. Harris and Allan G. Piersol. *Harris' Shock and Vibration Handbook*. McGraw-Hill Companies, Inc., 2002.

VITA

Naresh Kumar Koyyapu was born in Visakhapatnam, India. He was awarded First Class with Distinction in his Bachelor of Engineering (B.E.) degree in Mechanical (Marine as an Elective) Engineering from Andhra University, Visakhapatnam in March 2008. He also passed with Distinction in Master of Technology (M.Tech.) degree in Naval Architecture from Andhra University, Visakhapatnam in July 2012.

After his undergraduate degree, he joined Navarch Consultants & Engineers Pvt. Ltd. as Design Engineer and also executed key design projects in the role of Project Manager until March 2010. After that, he joined Demarc Marine Solutions Pvt. Ltd as Sr. Engineer (Naval Architect)/Project Manager. He enrolled in the graduate degree program at the University of New Orleans for Master of Science (M.S.) in Engineering with concentration in Naval Architecture and Marine Engineering in 2014. He started his career as an intern Naval Architect with Technology Associates, Inc. (New Orleans, LA) and working currently in the role of Naval Architect. He is currently the project engineer for the new design and build contracts for two foil assisted hydrographic survey catamarans for US Corps of Engineers (USACE).

He is an active member in professional societies *viz.,* The Society of Naval Architects and Marine Engineers (SNAME), USA and currently a Member in The Royal Institution of Naval Architects (MRINA), UK.